

SPD Learning for Covariance-Based Neuroimaging Analysis: Perspectives, Methods, and Challenges

Ce Ju[†], Reinmar J. Kobler[‡], Antoine Collas[†],
Motoaki Kawanabe[‡], Cuntai Guan[§], and Bertrand Thirion[†]



Abstract—Neuroimaging provides a critical framework for characterizing brain activity by quantifying connectivity patterns and functional architecture across modalities. While modern machine learning has significantly advanced our understanding of neural processing mechanisms through these datasets, decoding task-specific signatures must contend with inherent neuroimaging constraints, for example, low signal-to-noise ratios in raw electrophysiological recordings, cross-session non-stationarity, and limited sample sizes. This review focuses on machine learning approaches for covariance-based neuroimaging data, where often symmetric positive definite (SPD) matrices under full-rank conditions encode inter-channel relationships. By equipping the space of SPD matrices with Riemannian metrics (e.g., affine-invariant or log-Euclidean), their space forms a Riemannian manifold enabling geometric analysis. We unify methodologies operating on this manifold under the *SPD learning* framework, which systematically leverages the SPD manifold’s geometry to process covariance features, thereby advancing brain imaging analytics.

Index Terms—Geometric Statistics, Riemannian Geometry, Brain-Computer Interfaces, Neuroimaging

1 INTRODUCTION

NEUROIMAGING modalities, ranging from structural methods such as magnetic resonance imaging (MRI) and diffusion tensor imaging (DTI) to functional approaches such as functional magnetic resonance imaging (fMRI), electroencephalography (EEG), and magnetoencephalography (MEG), along with invasive recordings like electrocorticography (ECoG), naturally complement brain mapping and are valuable for characterizing mental health. In this review, we specifically focus on the analysis and learning methods for covariance-based neuroimaging data, which capture second-order statistics of neuroimaging signals, particularly covariance matrices derived from different neuroimaging modalities. For example, spatial covariance matrices in EEG are frequently used because they capture spatial relationships and synchronization between different regions of the

brain, which are essential for tasks such as motor imagery and emotion classification [1], [2]. Functional connectivity matrices derived from fMRI data are used to investigate cognitive-related disorders such as Alzheimer’s disease, schizophrenia, and multiple sclerosis [3], [4]. By analyzing these functional connectivity matrices, researchers can more precisely characterize interactions between functionally specialized brain regions, thus identifying biomarkers that inform the development of targeted diagnostic frameworks and therapeutic interventions [5], [6].

From a mathematical perspective, covariance-based neuroimaging data can be represented as SPD matrices, defined as $\mathcal{S}_{++}^n := \{S \in \mathbb{R}^{n \times n} \mid S^\top = S, \text{ and } x^\top S x > 0, \text{ for all } x \in \mathbb{R}^n \setminus \{0\}\}$. The space of SPD matrices forms a Riemannian manifold when equipped with a suitable mathematical structure. This geometric formulation ensures that the transformations and operations performed on SPD matrices remain within the manifold, preserving the intrinsic properties of the data. Therefore, statistical analysis of these covariance-based neuroimaging data naturally fits within the framework of geometric statistics, which combines statistical methods with concepts from differential geometry. Geometric statistics, in this context, originate from the analysis of DTI images, parallely advanced by two groups. While Fletcher and Joshi [7], [8] pioneered the application of affine-invariant Riemannian metrics [9] to SPD matrices for DTI analysis, Pennec, Fillard, and Ayache [10], [11] independently developed foundational Riemannian frameworks to process SPD manifold-valued data of tensor fields. This parallel development established the affine-invariant Riemannian metric as a standard Riemannian metric for SPD-based DTI statistics, enabling rigorous modeling and analysis of the variability in computational anatomy across many clinical research applications.

The space of SPD matrices forms a smooth manifold that fundamentally differs from Euclidean vector spaces due to its inherent geometric constraints. Crucially, SPD matrices are not closed under subtraction or negative scalar multiplication—operations that may yield symmetric matrices with non-positive eigenvalues, violating the SPD requirement. This necessitates specialized Riemannian metrics to properly handle manifold-valued data. Unlike the Euclidean metric,

[†] *Université Paris-Saclay, Inria, CEA, Palaiseau, France. (emails: {ce.ju, antoine.collas, bertrand.thirion}@inria.fr).*

[‡] *Advanced Telecommunications Research Institute International (ATR), Kyoto, Japan, and RIKEN Artificial Intelligence Project, Tokyo, Japan. (emails: {reinmar.kobler,kawanabe}@atr.jp).*

[§] *College of Computing and Data Science, Nanyang Technological University, Singapore. (email: ctguan@ntu.edu.sg).*

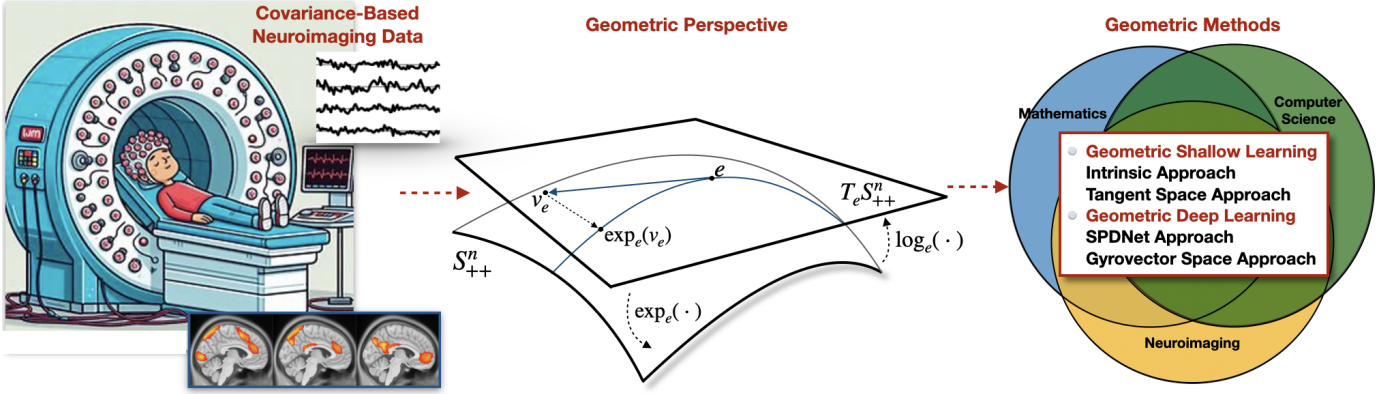


Fig. 1: SPD Learning Paradigm: different neuroimaging measurements, collected from neuroimaging techniques, are transformed into SPD matrices and considered as elements on an SPD manifold. The middle part of the diagram shows the SPD manifold S_{++}^n and its tangent space $T_e S_{++}^n$ at Fréchet mean e of SPD matrices, where v_e represents a tangent vector in the tangent space at e , and $\gamma(t)$ represents the geodesic passing through e . The tangent space at any point consists of all symmetric matrices of dimension $n(n+1)/2$. Specifically, the exponential map projects tangent vector v_e onto the SPD manifold as $\exp_e(v_e)$. On the far right, *SPD learning* refers to the collection of geometric methods applied on the SPD manifold in the perspective of geometric statistics. It is a subfield formed by the intersection of neuroimaging (M/EEG, fMRI, MRI, DTI, ECoG, etc.), computer science (signal processing, machine learning, statistical learning, deep learning, etc.), and mathematics (differential geometry, statistics, matrix theory, etc.).

which permits rank-deficient matrices at finite distances from SPD matrices (risking invalid intermediate results during optimization), the affine-invariant and log-Euclidean Riemannian metrics endow the SPD manifold with geodesic completeness. This property ensures: 1). Boundary avoidance: Geodesics between SPD matrices never reach boundary points (e.g., matrices with zero eigenvalues remain infinitely distant). 2). Intrinsic optimization: Iterative updates (e.g., gradient descent) stay strictly within the SPD manifold. These geometric guarantees resolve critical limitations of Euclidean-based tensor field processing, where conventional operations such as interpolation, regularization, or noise filtering often produce non-SPD matrices [10]. Consequently, medical imaging analysis increasingly adopts geometric statistics to handle manifold-valued data, enabling rigorous analysis on anatomical smoothing [12], fiber tractography [13], and disease biomarker extraction [14]–[16].

Inspired by the successful application of geometric statistics to DTI, representing fMRI connectivities as points on SPD manifolds offers an ideal parameterization. The tangent space parameterization provides a way to linearize the manifold, allowing conventional statistical techniques while minimizing the dependencies between the coefficients and respecting the inherent constraints of the SPD matrices [17]. In functional connectivity-based classification, the features derived from tangent space parameterization have been used effectively in classifiers, resulting in good decoding performance [18], [19]. Moreover, EEG spatial covariance matrices also have been conceptualized as points on SPD manifolds equipped with the affine-invariant Riemannian metric. Riemannian distances between covariance matrices derived from EEG signals serve as discriminative features for EEG-based motor imagery classification tasks, forming the foundation of the Riemannian-based classification framework [20]–[23]. The superior performance of this Riemannian-based classification framework stems from its capacity to preserve the intrinsic geometric properties of EEG covariance matrices while inherently encoding task-induced spectral

power modulations—specifically, event-related desynchronization/synchronization effects that characterize sensorimotor rhythm during motor imagery [24]–[26]. Compared to conventional EEG spatial filtering methods in EEG analysis, this Riemannian-based classification framework offers two advantages. First, it provides an intuitive, completely parameter-free approach to decoding by operating directly on covariance matrices in sensor space rather than estimating EEG spatial mixing matrix parameters from the source space. Second, it exhibits enhanced robustness against multi-source artifacts (e.g., bio-artifacts and environmental noise), which are critical characteristics for real-world EEG applications, and generality against distribution shifts across sessions and subjects that are typically due to the subject specificity of individual participants and variability across different sessions for the same participant. The success of this framework arises from two main factors: 1). the geometric mean’s inherent resistance to outliers, as demonstrated in both Gaussian and chi-square distributions where it deviates less significantly from distribution centers compared to the arithmetic mean; 2). the congruence invariance of the Riemannian distance, which holds regardless of changes in the EEG spatial mixing matrix across sessions and subjects [22]. Furthermore, recent work has extended the Riemannian-based classification framework to ECoG-based motor decoding, demonstrating robust classification of finger movement kinematics through spatial covariance patterns on manifolds [27]. The success of these methods across diverse neuroimaging modalities motivates our systematic evaluation of current *SPD learning* frameworks, with particular emphasis on identifying key challenges that remain unaddressed in real-world neuroimaging applications.

In this review, we will go through various analysis and learning methodologies applied to covariance-based neuroimaging tasks over the past twenty years. We collectively refer to these methods as *SPD learning* to address learning problems on SPD manifolds, particularly for neuroimaging tasks with covariance-based neuroimaging data. This term

encompasses a range of learning methods based on Riemannian geometry. Despite the different neurophysiological origins and acquisition mechanisms of various neuroimaging modalities, neuroimaging tasks often share inherent similarities. Unifying these learning methods by the term *SPD learning* is essential to optimize approaches in SPD manifolds. This unification promotes the use of geometric methods in the processing and the analyzing of covariance-based neuroimaging data. In addition, methods developed for specific neuroimaging tasks can inspire and be applied directly to other tasks, thus enhancing the versatility of neuroimaging data analysis.

The organization of this paper is as follows: In Section 2, we first introduce the concept of covariance-based neuroimaging data, which consists of two types of neuroimaging data. In Section 3, we cover Riemannian geometry, SPD manifolds, geometric statistics, and their applications in medical image analysis. Then, in Section 4, we introduce two categories of geometric methods for learning problems on SPD manifolds. In Section 5, we summarize the applications of *SPD learning* in various neuroimaging tasks. Afterward, we present the implementation toolkits in Section 6. Finally, we discuss the limitations and challenges of the current framework in Section 7.

2 COVARIANCED-BASED NEUROIMAGING DATA

In *SPD learning*, covariance-based neuroimaging data typically refer to second-order statistics derived from neuroimaging time series, such as EEG, MEG, ECoG, or fMRI. In addition, another type of data, commonly known as a tensor in medical image analysis, represents the image matrix within each voxel of an MRI image. Examples include the two types of covariance-based neuroimaging data which will be introduced in the following sections.

Time Series-Based Neuroimaging Data

Let $x(t) \in \mathbb{R}^{n_C}$ represent the neuroimaging signal at time t , where n_C denotes the number of spatial channels (e.g., brain regions or sensors). Preprocessing steps, such as bandpass filtering, centering, and scaling, are applied to $x(t)$. We assume approximate stationarity within short time windows, which is often applied to enable stable covariance estimation [28]. To construct a data segment $X \in \mathbb{R}^{n_C \times n_T}$, we concatenate the signals $x(t)$ into n_T consecutive time steps, so that $X := [x(t), x(t+1), \dots, x(t+n_T-1)]$. The *spatial covariance matrix* is defined as the expected outer product of the signal with itself: $\mathbb{E}[x(t)x(t)^\top] \in \mathcal{S}_{++}^{n_C}$. This matrix captures covariance across spatial channels, offering insight into spatial dependencies within neuroimaging data. It can be estimated using methods such as the empirical covariance matrix, the OAS estimator, and the Ledoit-Wolf estimator.

From a time-frequency perspective to explore the neuroimaging signal, we will consider the *cross power spectral density* (CPSD) of the time series. The CPSD at frequency f is defined as the Fourier transform of the covariance function, expressed as: $\int_{-\infty}^{\infty} \mathbb{E}[x(t)x(t+\tau)^\top] e^{-i2\pi f\tau} d\tau$. This function belongs to the set of Hermitian positive

definite matrices, capturing the frequency-dependent spatial structure of the signal. The CPSD thus describes how the power of the signal's spatial covariance is distributed across frequencies, enabling an examination of frequency-specific spatial interactions within the neuroimaging data. The CPSD can be computed using the Welch estimator, which provides a robust approach for spectral analysis by averaging over multiple overlapping segments of the time series.

In the discussion section, we provide more detailed considerations on covariance estimation and methods to address the issue when the covariance matrix may be singular (not full rank) and only positive semi-definite, e.g., when $n_T < n_C$. It is important to note that different neuroimaging modalities, such as EEG, MEG, ECoG, and fMRI, have varying temporal and spatial characteristics as well as distinct acquisition modalities. While constructing spatial covariance matrices and CPSD is common for modalities like EEG, MEG, and ECoG, applying the same approach to fMRI data requires careful consideration. The acquisition procedure of fMRI functional connectivity typically involves parcellating the brain into predefined regions and estimating the interactions between these parcels [29]. This process necessitates the use of different statistical and computational techniques to accurately capture the functional connectivity. For neuroimaging data such as EEG, MEG, ECoG, and fMRI, covariance-based neuroimaging data refer to the following descriptions.

- EEG/MEG/ECoG spatial covariance matrix: EEG and MEG are non-invasive neuroimaging techniques that measure electrical activity and magnetic fields generated by neural activity in the brain, respectively [30], [31]. ECoG, a type of intracranial electroencephalography, involves placing electrodes directly onto the exposed surface of the brain to monitor the electrical activity originating from the cerebral cortex [32]. While M/EEG operate non-invasively with sensor-level spatial resolutions of approximately 1 cm (EEG) and 3-5 mm (MEG), ECoG provides direct cortical access with millimetric precision, albeit at the cost of invasive implantation. Across these modalities, spatial covariance matrices quantify pairwise signal dependencies—either in sensor space (M/EEG) or source space (after inverse modeling)—serving as key descriptors of functional network interactions.
- fMRI functional connectivity/connectome: fMRI, a non-invasive method, measures brain activity by detecting changes in blood oxygenation levels, greatly enhancing our understanding of the functional organization underlying essential brain functions [33]. Functional connectivity in fMRI is often defined as temporal correlations between BOLD signal fluctuations in distant brain regions, measuring statistical dependencies in neural activity [34]. Covariance-based neuroimaging data are represented by functional connectivity matrices, also known as the connectome.

Tensor-Based Neuroimaging Data

Tensor-based neuroimaging data includes the diffusion tensor in DTI and the deformation tensor in MRI as follows.

- DTI diffusion tensor: DTI is a magnetic resonance imaging technique used to map and characterize the three-

dimensional diffusion of water molecules in biological tissues, which can reveal microstructural details such as white matter fiber tracts in the brain or muscle fiber structures [35], [36]. It estimates a diffusion tensor D at each voxel within the imaging volume, capturing the anisotropic diffusivity characteristics of water in that voxel. The diffusion tensor D is a 3×3 symmetric positive definite matrix that models the diffusion process and is estimated from diffusion-weighted MRI measurements using the Stejskal-Tanner equation $S_i = S_0 \exp(-bg_i^\top Dg_i)$, where S_0 is the signal intensity without diffusion weighting, and S_i is the measured signal with diffusion weighting along gradient direction g_i with diffusion factor b . The tensor D represents the principal diffusivities and directions of diffusion, providing insights into the underlying tissue microstructure.

- MRI Cauchy deformation tensor: MRI is a medical imaging technique that creates detailed images of the body's anatomy [37]. Statistical analyses of MRI data are crucial for identifying brain regions where anatomical properties differ between clinical groups or correlate with variables such as age, gender, medication, or genetic differences. To capture anatomical differences at a specific voxel X in MRI, the deformation fields obtained from image registration to a standard template are analyzed using the 3×3 Jacobian determinant $|J(X)|$. The Jacobian determinant at each voxel X quantifies the changes in local volume, thus providing a measure of anatomical variation. The MRI Cauchy deformation tensor at each voxel X is defined as $S := \sqrt{J(X)^\top J(X)}$.

3 GEOMETRIC PERSPECTIVES

Neuroimaging data when viewed as covariance matrices can be represented as SPD matrices. The collection of these SPD matrices forms a Riemannian manifold when equipped with an appropriate Riemannian metric. This allows for the statistical analysis of neuroimaging data to be approached from a geometric perspective. In this section, we introduce the basics of Riemannian geometry, which provides the foundational tools for geometric statistics and methods. We will then discuss some commonly used Riemannian metrics for SPD manifolds, along with general concepts in geometric statistics. Finally, we give an overview of key applications of geometric statistics in neuroimaging analysis. For a more detailed introduction to Riemannian geometry, see references [38]–[40].

3.1 Riemannian Geometry

Riemannian geometry is a branch of differential geometry focused on the study of Riemannian manifolds—smooth manifolds equipped with a Riemannian metric that defines the notions of distance, angle, and curvature on the manifold. A smooth manifold \mathcal{M} is a topological space that locally resembles Euclidean space. The tangent space $T_p\mathcal{M}$ at a point $p \in \mathcal{M}$ is a vector space consisting of tangent vectors to the manifold at any point $p \in \mathcal{M}$. It provides a linear approximation of the manifold near p . A vector field on a smooth manifold \mathcal{M} is a smooth map $X : \mathcal{M} \mapsto T\mathcal{M}$ that assigns to each point $p \in \mathcal{M}$ a tangent vector $X_p \in T_p\mathcal{M}$,

where $T\mathcal{M}$ denotes the tangent bundle of \mathcal{M} , representing the collection of all tangent spaces across \mathcal{M} .

A Riemannian manifold (\mathcal{M}, g) is a smooth manifold \mathcal{M} equipped with a Riemannian metric, which is symmetric positive-definite and smoothly varies with $p \in \mathcal{M}$. A Riemannian metric provides a means of quantifying geometric properties such as angles, curve lengths, areas, and volumes on Riemannian manifolds. Formally, it is given as follows:

Definition (Riemannian Metric). A Riemannian metric $g(\cdot, \cdot)$ at any $p \in \mathcal{M}$ is a smooth assignment of an inner product $g_p : T_p\mathcal{M} \times T_p\mathcal{M} \mapsto \mathbb{R}$ to each tangent space $T_p\mathcal{M}$, such that for any $u, v \in T_p\mathcal{M}$, the following properties hold:

- Positive-definiteness: $g_p(u, u) \geq 0$ and $g_p(u, u) = 0$ if and only if $u = 0$;
- Symmetry: $g_p(u, v) = g_p(v, u)$.

Moreover, g_p exhibits a smooth variation: given any two smooth vector fields X and Y , the inner product $g_p(X|_p, Y|_p)$ is a smooth function at p .

To connect local and global structures on manifolds, the Riemannian connection is introduced. This operation denoted as $\nabla_X Y$ describes how a vector field Y changes along another vector field X . The connection satisfies several key properties, such as linearity and compatibility with the Riemannian metric. It is uniquely defined on a Riemannian manifold and is often referred to as the Levi-Civita connection.

The Levi-Civita connection, denoted as $\nabla_X Y$, describes how a vector field Y changes along another vector field X . The connection satisfies several key properties, such as the compatibility with the Riemannian metric, and is uniquely defined on a Riemannian manifold. Let $\gamma : [0, 1] \rightarrow \mathcal{M}$ be a smooth curve, we say that a vector field X with respect to the Levi-Civita connection is parallel along γ if $\nabla_{\dot{\gamma}(t)} X = 0$ for all t . For any vector $v \in T_{\gamma(0)}\mathcal{M}$, there exists a unique parallel vector field X along γ with $X(0) := v$. The terminal value $X(1)$ is referred to as the parallel transport of v along γ , and it defines a linear map $P_\gamma : T_{\gamma(0)}\mathcal{M} \rightarrow T_{\gamma(1)}\mathcal{M}$. A geodesic is a curve $\gamma : [0, 1] \rightarrow \mathcal{M}$ such that its tangent vector $\dot{\gamma}$ is parallel transported along itself, i.e., $\nabla_{\dot{\gamma}} \dot{\gamma} = 0$. The Riemannian distance between two points $p, q \in \mathcal{M}$ is defined as the infimum of the lengths of all piecewise smooth curves joining p and q as $d(p, q) := \inf_\gamma \int_0^1 \|\dot{\gamma}(t)\|_g dt$, where the infimum is taken over all piecewise smooth curves $\gamma : [0, 1] \mapsto \mathcal{M}$ with $\gamma(0) = p$ and $\gamma(1) = q$.

The Riemannian exponential map is then introduced to enhance the comprehension of geodesics and their collective behavior. Formally, suppose that $v \in T_p\mathcal{M}$ is a tangent vector to each point $p \in \mathcal{M}$. Then there exists a unique geodesic γ_v that satisfies $\gamma_v(0) = p$ and $\dot{\gamma}_v(0) = v$. The exponential map is defined by $\exp_p(v) = \gamma_v(1)$. In particular, $\exp_p(0_p) = p$, where 0_p denotes the zero vector in $T_p\mathcal{M}$. There exists a neighborhood \mathcal{U} of 0_p in $T_p\mathcal{M}$ such that $\exp_p : \mathcal{U} \mapsto \mathcal{V}$ is a diffeomorphism onto its image $\mathcal{V} \subset \mathcal{M}$. The image of $\exp_p(T_p\mathcal{M})$ is called the exponential neighborhood of p . The radius of the largest ball centered at 0_p that is contained in \mathcal{U} is called the injectivity radius of \mathcal{M} at p . The exponential map is generally defined only in a local neighborhood of the tangent space based on a point on \mathcal{M} . They may not be globally well-defined unless the manifold possesses certain

TABLE 1: Basic operations on SPD manifolds equipped with AIRM and LEM, where $P, Q \in \mathcal{S}_{++}$ and $v, w \in \mathcal{T}_P \mathcal{S}_{++}$, \exp and \log are the matrix exponential and the logarithm, Tr is the trace of a matrix, and $D \log$ and $D \exp$ are the derivatives of \log and \exp , respectively.

Operator		AIRM	LEM
Inner Product	$\langle v, w \rangle_P$	$\langle P^{-\frac{1}{2}} v P^{-\frac{1}{2}}, P^{-\frac{1}{2}} w P^{-\frac{1}{2}} \rangle_{\mathcal{F}}$	$\langle D_P \log v, D_P \log w \rangle_{\mathcal{F}}$
Exponential Map	$\exp_P v$	$P^{\frac{1}{2}} \exp(P^{-\frac{1}{2}} v P^{-\frac{1}{2}}) P^{\frac{1}{2}}$	$\exp(\log P + D_P \log v)$
Logarithm Map	$\log_P Q$	$P^{\frac{1}{2}} \log(P^{-\frac{1}{2}} Q P^{-\frac{1}{2}}) P^{\frac{1}{2}}$	$D_{\log P} \exp(\log Q - \log P)$
Geodesic ($0 \leq t \leq 1$)	$\gamma_t(P, Q)$	$P^{\frac{1}{2}} \exp(t \log(P^{-\frac{1}{2}} Q P^{-\frac{1}{2}})) P^{\frac{1}{2}}$	$\exp((1-t) \log P + t \log Q)$
Geodesic Distance	$d(P, Q)$	$\ \log(P^{-\frac{1}{2}} Q P^{-\frac{1}{2}})\ _{\mathcal{F}}$	$\ \log P - \log Q\ _{\mathcal{F}}$

properties. For example, if \mathcal{M} is geodesically complete, meaning that every geodesic can be extended indefinitely in both directions, then the exponential map is globally defined. The inverse of the exponential map is called the logarithmic map. For any $q \in \mathcal{M}$ sufficiently close to p , the logarithmic map $\log_p(q)$ is defined as the unique tangent vector $v \in \mathcal{T}_p \mathcal{M}$ such that $\exp_p(v) = q$.

3.2 SPD Manifolds

The space of SPD matrices forms a smooth manifold that can be endowed with distinct Riemannian metric structures. Two canonical choices are the affine-invariant Riemannian metric (AIRM) [9], [10] and the log-Euclidean metric (LEM) [41], [42].

The AIRM, first formalized for SPD matrices by Pennec [9], exhibits critical invariance properties under congruence transformations. Specifically, for any non-singular matrix $W \in GL(n)$ and SPD matrices $P, Q \in \mathcal{S}_{++}$, the geodesic distance satisfies: $d_{g^{\text{AIRM}}}(WPW^T, WQW^T) = d_{g^{\text{AIRM}}}(P, Q)$. Formally, AIRM is defined at $P \in \mathcal{S}_{++}$ by $g_P^{\text{AIRM}}(v, w) := \langle P^{-\frac{1}{2}} v P^{-\frac{1}{2}}, P^{-\frac{1}{2}} w P^{-\frac{1}{2}} \rangle_{\mathcal{F}}$, where tangent vectors $v, w \in \mathcal{T}_P \mathcal{S}_{++}$. The Riemannian distance $d_{g^{\text{AIRM}}}(P, Q)$ is given by $\|\log(P^{-\frac{1}{2}} Q P^{-\frac{1}{2}})\|_{\mathcal{F}}$, where \log represents the matrix logarithm. The SPD manifold equipped with AIRM has the non-positive sectional curvature and is globally diffeomorphic to Euclidean space, with no cut locus. Furthermore, any two SPD matrices have a unique geodesic connecting them, and the Fréchet mean of a set of SPD matrices exists and is also unique. However, computations that involve this metric often experience slow performance because of the complexity of matrix operations. For example, obtaining the exact Fréchet mean on the SPD manifolds with AIRM requires an iterative method known as the Karcher flow to approximate the mean until the convergence conditions are met [43], [44].

The LEM simplifies the computations on the SPD manifold by utilizing the matrix logarithm to map this manifold to a Euclidean space. Specifically, the matrix logarithm $\log : \mathcal{S}_{++} \mapsto \mathcal{S}$ serves as a global diffeomorphism—a smooth, invertible map with a smooth inverse—between the SPD manifold and the vector space of symmetric matrices \mathcal{S} . By leveraging this mapping, the LEM is defined as the pull-back of the standard Euclidean metric under the logarithm. Formally, for any $P \in \mathcal{S}_{++}$ and tangent vectors v, w at P , the metric is given by $g_P^{\text{LEM}}(v, w) = \langle D_P \log v, D_P \log w \rangle_{\mathcal{F}}$, where $D_P \log$ denotes the differential of the logarithm at P . This construction means that computations on \mathcal{S}_{++} can be carried out in the logarithmic domain \mathcal{S} using standard Euclidean operations. As a result, many geometric proce-

dures, such as calculating distances, means, and interpolation between SPD matrices, become more tractable and efficient, which is particularly advantageous for statistical analyses in applications such as neuroimaging.

In addition to the two Riemannian metrics mentioned above, there are many other Riemannian metrics applied on \mathcal{S}_{++} , such as the Fisher information metric of elliptical distributions, the power Euclidean metric, the square root of log-det, the Log-Cholesky metric, the Bures-Wasserstein metric, the Thompson’s metric, and others [45]–[51]. However, since these Riemannian metrics are rarely applied in neuroimaging tasks, we will not explicitly include the details in this survey. Lastly, a summary of commonly used operations on SPD manifolds under the AIRM and LEM is provided in Table 1.

3.3 Geometric Statistics

Geometric statistics aims to extend fundamental statistical concepts such as the Fréchet mean, principal geodesic analysis, and geodesic regression to Riemannian manifolds [7], [8], [52]. This extension allows for the effective handling of statistical issues that arise from manifold-valued data in various applications [53]–[56]. For example, the Fréchet mean is determined by minimizing the sum of squared geodesic distances to the data points, and the Fréchet variance quantifies the dispersion of the data around the mean by measuring the average of these squared distances. These concepts facilitate the generalization of principal component analysis and regression to manifold settings, enabling more accurate and meaningful data analysis on Riemannian manifolds.

3.3.1 Fréchet Mean and Variance

The Fréchet mean and variance generalize the mean and variance to spaces equipped with a metric structure [57]. It is also known as the Karcher mean, often used interchangeably in the literature [58]. It should be noted that the Fréchet mean exists and is unique when the Riemannian manifold (\mathcal{M}, g) is complete with certain conditions involved with the sectional curvature and injectivity radius [59]. Formally, given a set of points $\{p_i\}_{i=1}^N$ on (\mathcal{M}, g) , the Fréchet mean μ is defined as the minimizer of the sum of squared Riemannian distances as $\mu := \arg \min_{p \in \mathcal{M}} \frac{1}{N} \sum_{i=1}^N d_g^2(p, p_i)$, which yields the following Fréchet variance σ defined as the expectation of the sum of squared Riemannian distances with respect to the Fréchet mean $\sigma^2 := \mathbb{E}[d_g^2(\mu, p)] = \frac{1}{N} \sum_{i=1}^N d_g^2(\mu, p_i)$. These two quantities serve as the basis for defining normal distributions on Riemannian manifolds. Specifically, such distributions are parameterized by μ and σ^2 , providing a natural extension of the concept of normality to manifold-valued data [60].

3.3.2 Principal Geodesic Analysis

To understand manifold-valued data, Principal Geodesic Analysis (PGA) was introduced to analyze the variance of the data by projecting it onto a series of nested geodesic submanifolds [7]. Formally, the empirical covariance matrix is given by $\frac{1}{N} \sum_{i=1}^N \log_{\mu}(p_i) \log_{\mu}(p_i)^{\top}$, where $\{p_i\}_{i=1}^N$ on (\mathcal{M}, g) are manifold-valued samples and μ is the Fréchet mean. Suppose that tangent vectors $\{v_i\}_{i=1}^N$ span the tangent space $\mathcal{T}_{\mu}\mathcal{M}$ at the Fréchet mean μ . One can construct a sequence of nested subspaces V_k by taking the span of the first k vectors in the set $\{v_i\}$. The principal geodesic submanifolds H_k are obtained by applying the exponential map $\exp_{\mu}(V_k)$ to V_k . The first principal direction is selected to maximize the projected variance along the corresponding geodesic as $v_1 := \arg \max_{\|v\|_g=1} \sum_{i=1}^N \|\log_{\mu}(\pi_H(p_i))\|_g^2$, where $H = \exp_{\mu}(\text{span}(v))$ and projection map $\pi_H : \mathcal{M} \mapsto H$ is defined as $\pi_H(p) := \arg \min_{x \in H} d_g^2(x, p)$. To define the remaining principal directions, a recursive approach is used by $v_k := \arg \max_{\|v\|_g=1} \sum_{i=1}^N \|\log_{\mu}(\pi_H(p_i))\|_g^2$, where $H = \exp_{\mu}(\text{span}(\{v_1, \dots, v_{k-1}, v\}))$. Several studies have developed algorithms for variance maximization formulas for Principal Geodesic Analysis (PGA) on specific or general Riemannian manifolds [61], [62]. In particular, if the original data is highly concentrated around the Fréchet mean, the PGA problem can be effectively approximated by the PCA optimization problem of points transformed by the Riemannian logarithm map, known as the tangent PCA approach [7].

3.3.3 Geodesic Regression

Geodesic regression is a generalization of linear regression on Riemannian manifolds seeking a geodesic that best fits the relationship between observed values y and regressors x . Formally, given $\{y_i\}_{i=1}^N$ on (\mathcal{M}, g) with an associated scalar $\{x_i\}_{i=1}^N \in \mathbb{R}$. For point $p \in \mathcal{M}$ and tangent vector $v \in \mathcal{T}_p\mathcal{M}$, the geodesic model, which is considered the generalization of multiple linear models on Riemannian manifolds, is given by $y = \exp_{\exp_p(xv)}(\epsilon)$, where \mathcal{M} -valued random variable y is an observation, the scalar $x \in \mathbb{R}$ is a regressor, and the random variable $\epsilon \in \mathcal{T}_{\exp_p(xv)}\mathcal{M}$ is the error term. Geodesic regression aims to find a geodesic $\gamma : [0, 1] \mapsto \mathcal{M}$ by minimizing the sum of squared Riemannian distance between all pairs of x_i and y_i , for $i \in \{1, \dots, N\}$, given by $\arg \min_{p, v} \frac{1}{2} \sum_{i=1}^N d_g(\exp_p(x_i v), y_i)^2$. For specific manifolds, geodesic regression can be solved analytically using Jacobi fields techniques [63].

3.4 Applications on Medical Image Analysis

The applications in medical image analysis have played a pivotal role in shaping and advancing the field of geometric statistics by addressing the complex data structures inherent in medical imaging.

3.4.1 DTI-Based Statistical Image Analysis

To address the measurement noise inherent in DTI images, various geometric statistical methods have been developed to process SPD manifold-valued data for purposes such as statistical estimation, smoothing, and interpolation [7], [8], [10], [11]. For example, Bayesian tensor estimation techniques have been employed to improve the accuracy of diffusion

tensor estimation in the presence of noise, especially in DTI images acquired from lower-quality scanners commonly used in clinical settings. These techniques often assume that the noise follows a Rician distribution and may utilize log-Euclidean parameterizations to facilitate computations [13]. Fillard et al. demonstrated that using the log-Euclidean framework can reduce the underestimation bias of tensor volumes compared to methods assuming Gaussian noise. Furthermore, regression models have been extended to SPD manifolds to address manifold-valued regression under the log-Euclidean metric and have been applied to the analysis of DTI diffusion tensors [64].

3.4.2 MRI-Based Tensor-Based Morphometry

The accurate assessment of changes in brain anatomy is essential to distinguish pathological variations from normal development and natural variability between populations. Tensor-based morphometry is a suitable method for analyzing these anatomical changes, as it calculates the spatial derivatives of deformation fields to align brain images with a standardized template. To effectively analyze deformation tensors derived from the Jacobian matrices of the deformation fields, such as the right and left Cauchy deformation tensors, which are SPD, geometric statistical approaches have been proposed that represent these tensors as points on the manifold of SPD matrices. This framework allows for the application of advanced statistical methods tailored for manifold-valued data. In the evaluation, appropriate statistical tests for SPD manifolds have been used to measure local anatomical differences between patients and control groups, providing more accurate and meaningful comparisons [65].

4 GEOMETRIC METHODS

A central objective in extending machine learning algorithms to SPD manifolds is to adapt classical Euclidean methods, such as K-means, nearest centroid classifiers, support vector machines, and neural networks, to function effectively within the manifold's structure. By incorporating Riemannian geometry, these algorithms can better exploit the non-Euclidean properties of SPD manifolds. In this section, we present a unified framework, referred to as *SPD learning*, designed to address learning challenges on SPD manifolds. This framework integrates geometric shallow learning with geometric deep learning techniques for a complete solution.

4.1 Geometric Shallow Learning (GSL)

Geometric shallow learning includes all non-deep learning methods adapted to SPD manifolds. These methods fall into two categories: intrinsic methods, which operate directly on the manifold by replacing Euclidean distances with Riemannian ones, and tangent space-based methods, which approximate the manifold by projecting data onto a unique tangent space, typically at the Fréchet mean, and then applying standard Euclidean machine learning algorithms.

4.1.1 Intrinsic Approach

Intrinsic methods leverage the manifold's geometry by systematically replacing Euclidean operations with their Riemannian counterparts. Key adaptations include geodesic

distances instead of Euclidean norms and Riemannian barycenters in place of arithmetic means. These principles extend to machine learning algorithms such as K-means clustering, nearest centroid classification, K-nearest neighbors, and support vector machines, which have all been reformulated for SPD manifolds. For example, kernel methods [66] can be defined with geodesic distances. Specifically, a Gaussian kernel on SPD manifolds is given by:

$$k(P, Q) := \exp\left\{\frac{-d^2(P, Q)}{2\sigma^2}\right\},$$

where $P, Q \in \mathcal{S}_{++}^n$, d denotes a Riemannian distance, and σ is the standard deviation. This approach preserves manifold geometry while enabling the direct use of kernel-based algorithms such as support vector machines, kernel PCA, and kernel K-means. Beyond Riemannian distances, information geometry provides alternative measures of discrepancy between SPD matrices using divergences such as the Kullback-Leibler divergence or the Jensen-Shannon divergence [67]–[70]. In addition, manifold learning further enriches intrinsic methods by reducing redundancy and alleviating the curse of dimensionality. Emerging in the early 2000s, these techniques aim to uncover low-dimensional representations of high-dimensional data while preserving their non-linear structure [71]–[73]. Specifically, SPD-aware frameworks, i.e. leveraging Riemannian distances, project high-dimensional SPD matrices onto lower-dimensional SPD manifolds while maintaining their geometric properties, avoiding distortions caused by Euclidean approximations [74], [75]. These advances have solidified intrinsic methods as a foundation for classification, clustering, and representation learning on SPD manifolds.

4.1.2 Tangent Space Approach

Tangent space mapping provides a practical approach to handling SPD manifolds by locally linearizing their geometry, typically at the Fréchet mean [20], [22], [76]–[78]. This transformation enables the direct application of standard machine learning methods without requiring algorithm-specific adaptations, as opposed to intrinsic approaches that rely on Riemannian distances and barycenters. Specifically, $Q \in \mathcal{S}_{++}^n$ is projected onto the tangent space at P via the logarithmic map associated with the affine invariant metric, transforming it into vectorized Euclidean features:

$$\begin{aligned} z &= \text{uvec}\left(P^{-\frac{1}{2}} \log_P(Q) P^{-\frac{1}{2}}\right) \\ &= \text{uvec}\left(\log\left(P^{-\frac{1}{2}} Q P^{-\frac{1}{2}}\right)\right) \in \mathbb{R}^{n(n+1)/2} \end{aligned}$$

where uvec encodes the upper triangular part with off-diagonal elements multiplied by $\sqrt{2}$. This mapping is chosen to preserve the Riemannian norm of the affine-invariant metric, i.e. $\|z\| = \|\log_P(Q)\|_P$. This approach allows the reuse of optimized Euclidean algorithm implementations. It has demonstrated strong performance by leveraging more expressive predictor models in the tangent space, whereas intrinsic approaches often require tailored, geometry-aware modifications [20], [77], [79].

4.2 Geometric Deep Learning (GDL)

Geometric deep learning is a rapidly evolving subfield of deep learning that focuses on analyzing data with non-

Euclidean structures, such as graphs and manifolds [80]. This approach has enabled significant advancements in diverse applications, including RNA structure prediction, molecular representation, and modeling microscopic motion [81]–[83]. Within the context of *SPD learning*, geometric deep learning extends the capabilities of deep neural networks to handle covariance-based neuroimaging data on SPD manifolds [84]–[87]. Two prominent frameworks have emerged for geometric deep learning on SPD manifolds: the SPDNet approach and the gyrovector space approach, which are introduced below.

4.2.1 SPDNet Approach

SPDNet is a deep neural network designed for classification tasks with SPD manifold-valued inputs [85]. SPDNet is trained using stochastic first-order optimization algorithms on manifolds, such as Riemannian SGD [88] and Riemannian Adam [89]. The gradient computations required for these algorithms are based on techniques for matrix-valued functions [90]. Its architecture consists of three types of layers as follows:

- 1). BiMap: This layer performs a bi-map transformation WSW^T on SPD matrix S , where W is the transformation matrix, typically required to have full row rank;
- 2). ReEig: This layer performs an eigenvalue rectification operation on S . Given the eigenvalue decomposition $S = U\Sigma U^T$, where U is an orthogonal matrix and Σ is a diagonal matrix, the output is computed as $U \max(\epsilon I, \Sigma) U^T$. Here, ϵ is the rectification threshold, and I is the identity matrix;
- 3). LogEig: This layer maps S to the tangent space at the identity matrix I using the Riemannian logarithm. Specifically, for $S = U\Sigma U^T$, the transformation is given by $U \log(\Sigma) U^T$, where $\log(\Sigma)$ is the element-wise logarithm of the diagonal entries of Σ .

To address the computational challenges of estimating the Fréchet mean on SPD manifolds, Brooks et al. [86] proposed a practical solution in their RieBN method. They utilized a fixed number of iterations of the Karcher flow algorithm during each forward pass. This network architecture approximately centers and re-biases batches of SPD matrices using parallel transport on SPD manifolds equipped with the affine-invariant Riemannian metric. Formally, given a batch of SPD matrices, RieBN performs batch centering and re-biasing using parallel transport operations as follows: $\Gamma_{\mathcal{B} \rightarrow e}(S_i) := \mathcal{B}^{-\frac{1}{2}} S_i \mathcal{B}^{-\frac{1}{2}}$ and $\Gamma_{e \rightarrow G}(\bar{S}_i) := G^{\frac{1}{2}} \bar{S}_i G^{\frac{1}{2}}$, where $\Gamma_{\mathcal{B} \rightarrow e}$ is the parallel transport from the batch Riemannian barycenter \mathcal{B} to the identity matrix e , and $\Gamma_{e \rightarrow G}$ is the parallel transport from e to a learnable bias parameter G . Here, \mathcal{B} represents the Fréchet mean of the batch.

To further enhance the accuracy of Fréchet mean estimation, Kobler et al. [91] introduced an efficient momentum-based technique. This approach updates the Fréchet mean during training, significantly accelerating convergence without requiring multiple Karcher flow iterations in mini-batches. Building on this, Kobler et al. [92] extended RieBN by incorporating the normalization of both the Fréchet mean and variance on SPD manifolds. This extension was inspired by insights into the role of batch normalization in Euclidean spaces [93] and demonstrated improved optimization landscapes, resulting in enhanced convergence and generalization

performance. More recently, Chen et al. [94] generalized RieBN to a broader class of Riemannian manifolds. Their method incorporates controlled normalization of sample and population statistics, further improving model robustness. These optimized versions of RieBN have consistently demonstrated superior performance compared to the original method in various applications.

4.2.2 Gyrovector Space Approach

The gyrovector space approach provides a principled framework for constructing deep neural networks on SPD manifolds by extending the theory of gyrovector spaces, originally developed for hyperbolic geometry [95], [96], to SPD, symmetric positive semidefinite (SPSD), and Grassmannian manifolds. This theory introduces operations such as gyro-addition and gyro-scalar multiplication, which, while analogous to Euclidean operations, are tailored to respect the intrinsic geometric properties of these manifolds.

In its early stages, gyrovector calculus was developed to create vector space analogs in curved spaces, alongside the introduction of vector-valued distances for computing metrics and extracting geometric insights from SPD manifolds [97]. Recent advances in gyrovector space methods have unified the understanding and application of matrix manifolds such as SPD, SPSD, and Grassmann manifolds. A key breakthrough is the definition of basic operations for different SPD geometries, including Affine-invariant, Log-Euclidean, and Log-Cholesky spaces, as well as their extension to low-rank SPSD manifolds via quotient geometry [98]. This flexibility has enabled new learning strategies for full- and low-rank settings, advancing recurrent neural networks for SPSD matrices.

Further contributions include gyro-isometries for SPD and Grassmann manifolds, preserving local structures while enabling deformations, which support geometric stability in deep learning. The introduction of the gyrohomomorphism, which generalizes linear transformations to gyro spaces, underpins neural networks invariant to isometries [99]. Additionally, gyrovector spaces have generalized fully connected and convolutional layers to SPD manifolds, enabled precise backpropagation with Grassmann logarithmic maps, and laid the foundation for graph convolutional networks on Grassmann manifolds, achieving remarkable results in tasks like human action recognition and node classification [100]. Another major leap came with the GyroAtt framework [101], which generalized the attention mechanisms to the gyrovector spaces in the SPD, SPSD, and Grassmann manifolds. Using geodesic distances for scoring and weighted Fréchet means for aggregation, GyroAtt demonstrated superior performance in EEG tasks, showcasing its flexibility and adaptability across various geometries.

5 NEUROIMAGING APPLICATIONS

In this section, we review the key applications of *SPD learning* to various neuroimaging tasks over the past twenty years. The review is organized by specific tasks, with different geometric methods presented for each of them. Table 2 provides a comprehensive list of the applications discussed in this section.

5.1 Motor Imagery Classification

In EEG-based motor imagery classification, EEG signals are collected while subjects engage in imagery tasks, such as imagining movements of the left hand, right hand, both feet, or tongue. Motor imagery involves mentally visualizing specific movements without physically performing them [144]. During this process, fluctuations in sensorimotor rhythms within the sensorimotor regions of the brain can serve as control signals for EEG-based BCIs [24]. When planning and executing movements, Sensorimotor rhythms show changes in amplitude known as event-related desynchronization/synchronization effects [25]. Event-related desynchronization indicates a decrease in rhythmic activity, whereas event-related synchronization indicates an increase. Since alterations in sensorimotor rhythms are visible in the band power of the signal, it is possible to enhance sensorimotor rhythm modulation by projecting the data into a subspace where the differences in band power between motor imagery classes are maximized.

Spatial filtering in EEG analysis involves the utilization of a spatial filter $W = [w_1, \dots, w_d] \in \mathbb{R}^{n_C \times d}$ to improve signal-to-noise ratios in the analysis of individual trials $x_t \in \mathbb{R}^{n_C}$ as $s_t = W^\top x_t$, where each electrode is weighted by the spatial filter $w_i \in \mathbb{R}^{n_C}$ to extract information about the true source of interest $s_t \in \mathbb{R}^d$, n_C is the spatial dimension of EEGs and d is the reduced dimension. This is because the EEG signal recorded at an electrode not only reflects neural voltage fluctuations that electrode but also captures the activity of distant current sources through volume conduction effects [145].

Spatial Covariance Matrix-based Feature

The common spatial pattern (CSP) method, which inputs EEG spatial covariance matrices as classification features, is one of the most widely used spatial filtering techniques in motor imagery tasks [1]. It aims to identify the direction that maximizes the variance between the average EEG spatial covariance matrices of two classes of motor imagery through simultaneous diagonalization. After simplification, spatial filters w_i in the common spatial pattern method are acquired by solving the generalized eigenvalue problem $\Sigma^+ w_i = \lambda_i \Sigma^- w_i$, where Σ^+ and $\Sigma^- \in \mathbb{R}^{n_C \times n_C}$ are two average spatial covariance matrices of two classes, λ_i represents the generalized eigenvalue, representing the variance ratio between two classes, for all $i \in \{1, \dots, n_C\}$. This approach has several variants that are applicable in various scenarios and has been successfully applied in various online BCI systems [26].

The CSP method can be formulated as a divergence maximization problem from the perspective of information geometry. Studies [113], [114] demonstrated that the subspace spanned by the top- d CSP spatial filters $W \in \mathbb{R}^{n_C \times d}$ maximizes the symmetric Kullback-Leibler divergence $\bar{\mathcal{D}}_{KL}$ between Gaussian distributions of the form $\mathcal{D}_{KL}(\mathcal{N}(0, W^\top \Sigma^+ W) \parallel \mathcal{N}(0, W^\top \Sigma^- W))$. This insight provides an alternative way to obtain the CSP subspace by directly maximizing divergence, rather than solving a generalized eigenvalue problem. Furthermore, by incorporating various regularization terms and beta divergence techniques between distributions, the divCSP framework unifies several CSP variants in a principled manner.

TABLE 2: List of Applications of SPD learning on Neuroimaging Tasks.

Neuroimaging Task	Modality	Method	Literature Review
5.1 Motor Imagery Classification	EEG	GSL GDL	[20]–[22], [102]–[114] [91], [92], [115]–[121]
5.2 Emotion Classification	EEG	GDL	[122]
5.3 SSVEP Classification	EEG	GSL	[123], [124]
5.4 Finger Movement Classification	ECoG	GSL	[27]
5.5 Multimodal Fusion	Simultaneous EEG-fMRI	GDL	[125]
5.6 Representation of Brain Functional Dynamic	fMRI	GDL	[126]
5.7 Aging Prediction	M/EEG	GSL	[127]–[130]
	fMRI, MRI, MEG, etc.	GSL	[77]–[79], [108], [131]–[133] [134]–[136]
5.8 Neuropsychological Disorder Prediction	fMRI	GSL	[16]–[19], [137], [138]
	MRI	GSL	[139]–[142]
		GDL	[143]

From the standpoint of Riemannian geometry, motor imagery classification can benefit from using the Riemannian distance between EEG spatial covariance matrices—viewed on SPD manifolds—by comparing each matrix to the Fréchet mean of its corresponding class, a strategy referred to as the Riemannian-based approach [20]–[22]. This unified framework streamlines conventional EEG processing pipelines by merging pre-processing and feature extraction into a single stage prior to classification, thereby enhancing classification performance across various paradigms [22].

Moreover, manifold learning techniques have been developed to embed high-dimensional SPD matrices into lower-dimensional spaces while preserving local data structure and incorporating supervised information. For instance, one approach to Riemannian manifold embedding seeks to obtain lower-dimensional representations by minimizing the weighted total squared Riemannian distance between SPD matrices, measured using affine-invariant Riemannian metrics between each pair of embeddings [110], [111]. In the same year, an alternative method was proposed that instead maximizes the weighted total squared Riemannian distance for dimensionality reduction on SPD manifolds [112].

The latest category of EEG-based motor imagery classifiers, known as geometric classifiers [118], leverages deep neural networks on SPD manifolds to extract discriminative information from EEG spatial covariance matrices across time, space, and frequency domains. Essentially, these classifiers extend the CSP classifier into a deep neural network framework via the SPDNet approach. For example, the BiMap layer in SPDNet functions as a data-driven spatial filter, with its weights updated through matrix backpropagation during training. Specifically, each learned column weight w of the transformation matrix W in the BiMap layer lies on the Stiefel manifold $V_{nc}(\mathbb{R}^{nc})$. The key difference lies in how the weight w is obtained: the CSP method obtains w by solving a simultaneous diagonalization problem, while the SPDNet approach learns it by the matrix backpropagation directly from data. Furthermore, the SPDNet architecture incorporates a non-linear ReEig layer along with a LogEig layer that performs operations analogous to the logarithmic transformation used in CSP methods. Together, these mechanisms enable SPDNet to customize the spatial filtering process to the specific characteristics of the EEG data, potentially leading to more robust and accurate classifications.

The initial geometric classifier, Tensor-CSPNet [116], segments EEG signals into short time-frequency intervals

and computes the spatial covariance for each segment. These covariance matrices are then arranged into four-dimensional tensors, which are sequentially processed across the time, frequency, and spatial dimensions using neural networks operating on SPD manifolds. Building on this foundation, Graph-CSPNet [118] simultaneously extracts discriminative information from both the time-frequency and spatial domains, using spectral clustering to effectively manage irregular EEG segments and enhance segmentation flexibility. In parallel, the Riemannian embedding bank [115] refines SPDNet by incorporating deep metric learning techniques. It partitions both the EEG data and the embedding space into non-overlapping subsets, thereby enabling the independent learning of distinct distance metrics on SPD manifolds for each subset. Additionally, Pan et al. [117] introduce a manifold attention mechanism into SPDNet that leverages the log-Euclidean metric to more effectively capture temporal dynamics. Furthermore, a recent study [121] investigates how SPDNet can be enhanced through the integration of learnable filterbanks—a significant departure from the prevailing reliance on pre-defined filterbanks in existing literature. This work systematically evaluates key parameters, such as filter type, channel specificity, and filterbank size, to determine their impact on classification performance and to uncover neurophysiologically relevant insights. Ultimately, it assesses whether SPDNet equipped with learnable filterbanks can match or even surpass state-of-the-art EEG decoding techniques. Collectively, these innovations push forward the capabilities of geometric classifiers for EEG by harnessing the inherent structure of SPD matrices and integrating advanced deep learning strategies.

Multivariate Time Series-based Feature

The fact that motor imagery results in distinct power modulations in canonical sensorimotor rhythms inspired many spectrally resolved approaches from the classic common spatial pattern method up to the recent geometric classifiers [116], [118]. These approaches utilize prior knowledge to extract features of the spatial covariance matrix resolved spectrally with predefined filter banks. Motivated by the success of deep learning, recent works introduced learnable convolutional feature extractors instead of predefined filter banks [117], [146], [147]. For instance, an inherently interpretable architecture called TSMNet combines a linear convolutional feature extraction layer with covariance pooling, SPDNet, and RieBN to learn classic tangent space models on $(S_{++}, g^{\text{AIRM}})$ in an end-to-end fashion [146]. In the same year, the work that

proposed the SPDNet-based manifold attention mechanism reported the highest performance gains if a convolutional feature extractor precedes SPDNet [117]. Lastly, Wilson et al. provide a detailed analysis of the interaction between convolutional and subsequent SPDNet layers in the context of motor imagery [147].

Domain Adaptation Problem

The nonstationary characteristics of EEG signals introduce substantial variability across multiple dimensions, including within-session fluctuations, cross-session discrepancies, and pronounced inter-subject differences [148]. This variability frequently manifests as distributional shifts across domains—such as sessions, subjects, or recording configurations—which has spurred the development of specialized domain adaptation methodologies for SPD manifolds.

A foundational approach involves geometry-aware alignment through parallel transport under the affine-invariant Riemannian metric. By translating data clusters to the Fréchet mean of the dataset, this technique harmonizes inter-domain distributions and has demonstrated efficacy in EEG signal processing applications [105], [149]. Building upon these geometric principles, the Riemannian Procrustes analysis extends classical statistical shape alignment to SPD manifolds by incorporating geometric transformations such as translation, scaling, and rotation. This framework enables systematic distribution alignment while preserving the intrinsic structure of the manifolds [104], [107], [150]. For scenarios involving dimensional mismatch between experimental setups, dimensionality transcending methods first project data to a common latent space through dimensionality alignment, then apply Riemannian Procrustes analysis for statistical distribution matching—effectively addressing cross-configuration variability [106].

Recent innovations have introduced physics-informed approaches to handle channel configuration disparities. Electromagnetic field interpolation maps EEG channels to standardized spatial coordinates based on neurophysical principles. When integrated into Riemannian classification pipelines, this method outperforms traditional approaches in low-channel-overlap scenarios by leveraging biophysical constraints [108]. In parallel, recent work has explored the application of optimal transport on SPD manifolds to capture the intricate structure of M/EEG signals. By introducing a Sliced-Wasserstein discrepancy specifically designed for SPD matrices, the approach efficiently quantifies the differences between the distributions of covariance matrices derived from brain recordings [109].

Deep learning adaptations have further expanded the methodological toolkit. Log-Euclidean optimal transport reformulates distribution alignment as a joint adaptation problem on SPD manifolds, simultaneously matching marginal and conditional distributions to address session variability [119]. Meanwhile, federated learning frameworks reconcile privacy constraints with cross-subject adaptation by aggregating EEG covariance matrices into a shared SPD subspace while maintaining subject-specific parameters [120]. These coordinated advances—spanning geometric transformations, biophysical modeling, and deep architecture innovations—collectively address the multifaceted challenges of

EEG variability through principled Riemannian manifold operations. Complementing these geometric strategies, domain-specific SPD batch normalization adapts translation and scaling operations from Riemannian Procrustes analysis for deep learning frameworks. This learnable module effectively mitigates cross-session and cross-subject variability through end-to-end distribution alignment [146].

5.2 Emotion Classification

EEG is widely used to investigate cognitive and emotional processes in humans, mainly due to the predictive power of cerebral asymmetry in relation to affective responses, emotional valence, and personality traits [151]. Research in psychophysiology shows a clear correlation between neural activity in the left and right frontal lobes and specific emotional states. Increased activity in the left frontal region is associated with positive emotions, while increased activity in the right frontal region correlates with negative emotional states [2]. A recent study used SPDNet to capture emotional representations in multiple contexts. This architecture, known as the Domain Adaptation SPD Matrix Network, integrates prototype learning with a novel prototype loss function, leading to enhanced performance in emotion recognition [122].

5.3 SSVEP Classification

In the steady-state visually evoked potential paradigm based on EEG, participants focus on stimuli flashing at different frequencies, generating brain waves that are phase-locked and frequency-matched to the stimulus. These signals are modulated by the participant’s attention [152]. SSVEP classification typically involves identifying the stimulus-specific frequency in the visual cortex. Canonical correlation analysis is a common method used for this task, as it identifies the stimulus frequency that exhibits the highest correlation with brain signals [153]. Recently, geometry-aware methods have been introduced to address variability in synchronous and online SSVEP classification. These methods, combined with transfer learning, effectively mitigate intersubject variability, leading to improved classification accuracy [123], [124].

5.4 Finger Movement Classification

ECoG offers higher bandwidth and spatial resolution compared to EEG, enabling more precise decoding and more intuitive control in brain-machine interfaces [154]. For example, the decoding of five-finger movements has been enhanced by adapting a Riemannian-based classification framework originally designed for EEG-based motor imagery classification to work with ECoG spatial covariance matrices. This approach leverages sparse representations of Riemannian biomarkers, achieving accurate decoding of motor activity from ECoG signals [27].

5.5 Multimodal Fusion

Various non-invasive imaging techniques provide unique insight into brain functions and structures. To take advantage of the rich information from these diverse modalities, it is essential to integrate them effectively through multimodal

fusion. This fusion aims not only to extract shared characteristics between different modalities but also to capture distinct and complementary characteristics unique to each modality [155]. For example, integrating neuroimaging approaches that combine simultaneous EEG and fMRI holds promise in improving our understanding of brain functional connectivity by leveraging the high temporal resolution of EEG and the high spatial resolution of fMRI [156], [157]. However, differences in time scales, spatial resolutions, and physiological signals measured by EEG and fMRI pose significant challenges to achieve consistent and meaningful integration of data from each modality [158].

In a recent study, a novel approach named Deep Geodesic Canonical Correlation Analysis [125] has been proposed to learn a shared SPD manifold-valued latent representation for covariance-based neuroimaging modalities, specifically EEG spatial covariance matrices and fMRI functional connectivity matrices. By aligning the representations of both modalities on the SPD manifold, this approach maximizes their geodesic correlation, effectively capturing their intrinsic relationships. The learned latent space enables better integration of EEG and fMRI data, enhancing multimodal fusion. Finally, when applied to downstream motor imagery classification, this method exhibits superior generalization, achieving statistically significant improvements in accuracy over classifiers trained on individual modalities.

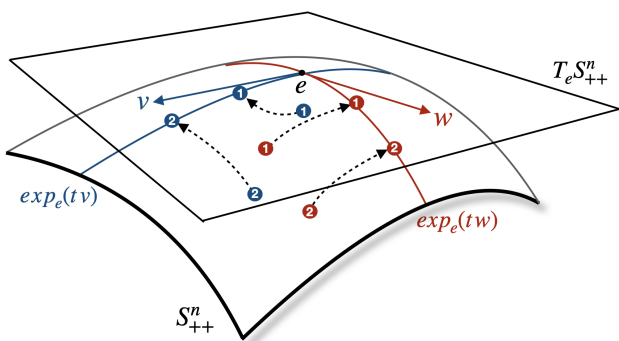


Fig. 2: Geodesic Correlation on SPD Manifolds [125]: A generalized statistical correlation specifically for covariance-based neuroimaging data is quantified by calculating the correlation between tangent vectors, which represent manifold-valued data projected onto the respective geodesics of the tangent spaces of each modality at the identity element e . In the figure, two pairs of SPD manifold-valued data labeled as 1 and 2 from two modalities are first orthogonally projected onto the geodesics $\exp_e(tv)$ and $\exp_e(tw)$, and then the correlation is computed using the pairs of orthogonal projections.

5.6 Representation of Brain Functional Dynamic

Recent fMRI research has increasingly focused on functional dynamics, as growing evidence indicates that brain activity fluctuates even during rest periods. Consequently, understanding brain function requires characterizing the evolving network structure of fMRI functional connections [159]. In earlier studies, the Riemannian metric derived from transported square-root vector fields was shown to be invariant under re-parameterization groups, enabling rate-invariant analysis of dynamic functional connectivity trajectories [160]. Additionally, utilizing this Riemannian metric allows for the registration, comparison, and classification of the tangent

bundles of SPD manifolds with respect to dynamic functional connectivity trajectories [126].

Several recent studies incorporate the BiMap layer from SPDNet, enabling data-driven transformations of dynamic functional connectivity matrices. This enhances the understanding of dynamic functional connectivities by capturing local geometric patterns associated with underlying states, known as spectral or shape signatures, related to brain resting states on SPD manifolds [127]–[130]. For instance, CPD-Net introduces a task-specific functional connectivity fingerprint as the loss function to detect transition points between fMRI tasks [127]. Another study proposes an SPD manifold-valued convolutional neural network, augmented with a geometric attention mechanism and a recurrent neural network, to learn latent representations of the temporal relationships captured by dynamic functional connectivity trajectories on SPD manifolds [128]. Furthermore, Geo-Net4Net has been developed to extract intrinsic low-dimensional representations of functional connectivities derived from resting-state functional brain networks [129]. Additionally, the latest study by the same research group introduces a physics-informed deep model to explore the connection between brain structure and function. The model leverages data geometry based on the extensive network of connections between distant brain regions [130].

5.7 Aging Prediction

The aging brain undergoes characteristic structural and functional reorganization, marked by volumetric reductions and declining cognitive capacities. Neuroimaging studies reveal distinct connectivity patterns: resting-state networks exhibit weakened intra-network synchronization alongside strengthened inter-network coupling over time [161]–[164]. These dynamics position M/EEG and fMRI as critical tools for mapping lifespan neural trajectories.

For M/EEG paradigms, low-rank spatial covariance matrices have emerged as robust descriptors for age prediction, circumventing anatomical variability without requiring explicit source modeling [77], [78]. To enhance cross-domain generalizability, geometric alignment techniques—recentering, scaling, and rotational adjustments—compensate for session-specific variations in neurophysiological signals and sensor configurations. The Geodesic Optimization for Predictive Shift Adaptation (GOPSA) framework synergistically learns domain-invariant transformations and regression models, achieving state-of-the-art performance in multinational EEG studies (14 sites, $N > 1500$), particularly under heterogeneous data distributions [79], [132], [133].

In fMRI-based aging research, sparse inverse covariance matrices representing functional networks are embedded into SPD manifolds via locally linear projections. The log-Euclidean metric enables efficient manifold learning, outperforming Euclidean approaches in capturing lifespan network reconfiguration. Ridge regression within this geometric space identifies progressive cortical-subcortical integration in sensorimotor systems and segregation in frontoparietal/emotional networks across adulthood [134].

Multimodal integration further advances predictive precision: Liem et al. developed a unified model integrating

cortical thickness, surface area, subcortical volumes, and functional connectivity (197/444 parcellations) across 2,354 adults. Their multimodal approach achieved a mean absolute brain-age error of 4.29 years—surpassing unimodal benchmarks—while demonstrating resistance to head motion artifacts and cross-site generalizability. Notably, the brain-age gap (predicted vs chronological age) reliably tracked cognitive impairment severity, validating its potential as a transdiagnostic biomarker in neurodegenerative disorders [135].

Complementing these efforts, combining MEG spectral power (8-30 Hz dominance), MRI morphometrics, and fMRI connectivity in the Cam-CAN cohort (N=674) yields additive explanatory power for age-related cognitive decline. Critically, this framework maintains robustness against missing modalities, preserving its utility in clinical settings with incomplete data [136].

5.8 Neuropsychological Disorder Prediction

Many research studies have demonstrated that fMRI functional connectivity is effective in identifying neuropsychological disorders such as Alzheimer’s disease, autism spectrum disorder, depression, Parkinson’s disease, and schizophrenia [165]–[167]. Representing fMRI functional connectivity on SPD manifolds provides a robust parameterization method known as tangent-space parameterization [17]. In classification tasks based on functional connectivity, this parameterization is utilized as a feature for classifiers, leading to strong decoding performance [18]. Another study evaluated the strengths and limitations of predictive models based on fMRI functional connectivity. The investigation considered various factors both independently and jointly, including: parcellation techniques, measures of functional connectivity, shrinkage estimators, dandling confounds, classifiers, and predictors. All models were assessed using resting-state fMRI datasets from the UK Biobank and the Human Connectome Project [19]. Furthermore, a study utilized Riemannian geometric frameworks to preserve the mathematical properties of functional connectomes during harmonization. The research demonstrated how state-of-the-art harmonization methods can be integrated within these frameworks to reduce the effects of covariates while maintaining relevant clinical information related to aging or brain disorders. Experiments confirmed that the new framework successfully harmonized both low-dimensional connectomes and voxel-wise functional time series. This underscores the importance of preserving connectome properties during harmonization [16].

Longitudinal data-driven models in neuroimaging are employed to study the progression of age-related brain diseases, such as Parkinson’s and Alzheimer’s disease [168], [169]. These models estimate continuous subject-specific trajectories, aligning them across both spatial regions and temporal points to monitor disease progression accurately. In a study focused on classifying fMRI connectivity before and after interventions in longitudinal studies, a matrix whitening transport method was proposed to project covariance estimates onto a common tangent space, thereby reducing statistical dependencies between their elements [137], [138]. This approach achieved significantly higher classification

accuracy and identified several neuroanatomically significant connections.

To address manifold-valued neuroimaging measurements, statistical models like the mixed-effects model have been extended to Riemannian manifolds [139]. This geometry-aware method introduces parallel curves on manifolds to decompose observed differences in the data into spatial and temporal components. The manifold-valued mixed-effects model is further generalized to a Bayesian framework to estimate the temporal progression of biological phenomena based on repeated observations across a group of individuals [142]. Additionally, a semi-parametric geometric approach has been proposed, utilizing a reproducing kernel Hilbert space to estimate the Riemannian metric, thereby capturing inter-individual variability in patient trajectories within the mixed-effects model [141]. Another study expanded non-linear mixed-effects models into a Riemannian framework to handle responses on curved spaces [140]. By interpreting the non-linear transformations between successive time points as Cauchy deformation tensors, this method enables longitudinal analysis that aligns with the geometric nature of deformation data.

Recently, a geometric deep learning-based model was introduced to model Alzheimer’s disease prognosis using structural MRI features. Their approach incorporates a convolutional feature extractor, covariance pooling, and a recurrent layer on the SPD manifold equipped with the Log-Cholesky metric. To address the common issue of missing longitudinal observations, the researchers employed a neural manifold ordinary differential equation to estimate the latent trajectory, enhancing the robustness of the prognostic model [143].

6 IMPLEMENTATIONS

This section reviews the manifold-valued optimizers based on Riemannian optimization and open-source software packages to implement *SPD learning*.

6.1 Manifold-Valued Optimizers

In *SPD learning*, many of the model parameters are manifold-valued, which requires the use of manifold-valued optimizers for effective optimization in these curved spaces. In mathematics, there is a specialized research field dedicated to studying such optimization problems called Riemannian optimization [170], [171]. It addresses optimization problems in Riemannian manifolds, that is, $\min_{x \in \mathcal{M}} f(x)$, where \mathcal{M} denotes a Riemannian manifold and $f : \mathcal{M} \mapsto \mathbb{R}$ is the objective function. The classical gradient descent adapts to manifolds using a retraction operator $R_P : \mathcal{T}_P \mathcal{M} \mapsto \mathcal{M}$ at any point $P \in \mathcal{M}$ to iteratively map the updated points along the direction of the Riemannian gradient ∇f to the manifold, given by $x_{k+1} \leftarrow R_{x_k}(-\alpha_k \nabla f(x_k))$, where $\alpha_k > 0$ is the step size at x_k .

In neural network-based models, conventional stochastic gradient descent has been extended to Riemannian manifolds to update network weights, with convergence analyzes conducted in various settings [88], [172]. Recently, several adaptive optimization schemes, such as Adam [173], AdaGrad [174], and AMSGrad [175], have been adapted for manifold optimization. These adaptations include convergence analyzes specifically tailored to geodesically convex

scenarios [89]. Variance-reduced Riemannian optimization algorithms have also been proposed in order to achieve faster convergence to minimize finite sums of geodesically smooth convex and nonconvex functions on Riemannian manifolds [176]. Additionally, a modified approach using Riemannian normal coordinates has been proposed to ensure that each iteration remains on the submanifold. This method dynamically orthonormalizes the metric, effectively transforming the problem locally into an unconstrained optimization task in Euclidean space [177].

6.2 Open-Source Software Packages

Open-source software packages for deterministic Riemannian optimization are provided by `pymanopt`¹, `manopt`², `Manopt.jl`³, and `Manifolds.jl`⁴ [178]–[181]. All packages support the SPD manifold, with manual specification of gradients and Hessians in `manopt` and automatic differentiation in `pymanopt` and `Manopt.jl/Manifolds.jl`, as well as solvers for unconstrained cost functions. The `Manopt.jl/Manifolds.jl` package additionally provides solvers for non-smooth and constrained optimization problems [180]. The Python packages `geoopt`⁵ and `geotorch`⁶ offer an alternative with stochastic optimization for deep learning based on the PyTorch framework [182], [183]. They support popular Riemannian manifolds, including the SPD manifold with the affine invariant Riemannian metric, and popular deep learning optimizers like Adam.

More advanced *SPD learning* are mainly supported by two open-source Python packages. First, the `geomstats`⁷ project provides an open-source Python package for computations, statistics, and machine learning on Riemannian manifolds and Lie groups [184]. The package offers a user-friendly API similar to `scikit-learn` and supports Fréchet means, clustering, shallow geometry-aware classification, and geodesic PCA. In particular, the `Information Geometry` module [185] implements the Riemannian geometry of the SPD manifold with the affine invariant metric. Then, the `pyRiemann`⁸ package provides preprocessing and machine learning tools for real and complex-valued data through computations on the SPD manifold [186]. The provided preprocessing tools include spectrally-resolved covariance estimation and regularization methods. It supports popular Riemannian metrics proposed for the SPD manifold and comes with tutorials for EEG, including artifact detection and correction, classification, statistical testing, and transfer learning. On top of these two libraries, `scikit-learn` [187] provides essential machine learning algorithms and evaluation metrics through a consistent API, enabling seamless integration of *SPD learning* algorithms with standard machine learning pipelines. In addition, the software landscape for geometric deep learning methods is fragmented. Reference implementations of recently pro-

posed methods are available for Tensor-/Graph-CSPNet⁹, TSMNet¹⁰, MAtt¹¹, SPDMLR¹², LieBN¹³, and GREEN¹⁴.

In the context of neuroimaging, `MNE-Python` [188] provides the basic neurophysiological data processing tools for EEG and MEG signals such as artifact removal, filtering, source localization, time-frequency analysis, and statistical analysis of sensor and source space data. The `Nilearn`¹⁵ package offers various statistical and machine learning tools dedicated to fMRI [189] such as connectivity analysis, functional parcellation, and advanced visualization of brain volumes. Its support for *SPD learning* is limited to tangent space for SPD manifold equipped with AIRM.

7 CHALLENGES

In this section, we identify three key challenges for *SPD learning*: covariance estimation, matrix computation, and interpretability. Through a systematic review of existing solutions, we not only present current research progress but also aim to illuminate pathways for future optimization. Because a careful consideration of these factors in the implementation will bring more stability, reliability, and efficiency.

7.1 Covariance Estimation

Estimating covariance matrices from limited observational data remains a persistent challenge in real-world applications [190], [191]. While the empirical covariance matrix serves as an unbiased and consistent estimator, its reliability degrades significantly in high-dimensional, low-sample regimes, exhibiting heightened sensitivity to outliers. This issue manifests acutely in domains such as fMRI functional connectivity analysis and Gaussian modeling of brain interactions, where covariance dimensions frequently surpass available sample sizes, resulting in unstable estimations [192]–[194]. For instance, neuroimaging studies often face covariance matrices with thousands of variables but merely hundreds of observations, exacerbating the small-sample problem.

To address these limitations, statisticians have developed regularization strategies for high-dimensional covariance estimation, notably shrinkage methods and sparsity-inducing techniques. A landmark advancement is the Ledoit-Wolf shrinkage estimator [195], which stabilizes the sample covariance through a convex combination with a structured target matrix. This approach guarantees positive definiteness, improves conditioning, and achieves asymptotic superiority over conventional sample covariance estimators [196]. Such regularization frameworks have proven instrumental across neuroimaging workflows, enhancing covariance estimation for critical tasks including predictive regression, disease classification, and population-level statistical inference [197]–[200].

1. `pymanopt`: <https://github.com/pymanopt/pymanopt>
2. `manopt`: <https://github.com/NicolasBoumal/manopt>
3. `Manopt.jl`: <https://github.com/JuliaManifolds/Manopt.jl>
4. `Manifolds.jl`: <https://github.com/JuliaManifolds/Manifolds.jl>
5. `geoopt`: <https://github.com/geoopt/geoopt>
6. `geotorch`: <https://github.com/lezcano/geotorch>
7. `geomstats`: <https://github.com/geomstats/geomstats>
8. `pyRiemann`: <https://github.com/pyRiemann/pyRiemann>

9. Tensor-/Graph-CSPNet: <https://github.com/GeometricBCI/Tensor-CSPNet-and-Graph-CSPNet>
10. TSMNet: <https://github.com/rkobler/TSMNet>
11. MAtt: <https://github.com/CECNL/MAtt>
12. SPDMLR: <https://github.com/GitZH-Chen/SPDMLR>
13. LieBN: <https://github.com/GitZH-Chen/LieBN>
14. GREEN: <https://github.com/Roche/neuro-green>
15. Nilearn: <https://github.com/nilearn/nilearn>

Alternatively, sparse covariance estimators offer an alternative regularization approach, exemplified by graphical lasso methods that enforce sparsity in covariance or precision matrices to recover conditional independence structures [201]. Nevertheless, these sparsity-centric estimators face fundamental limitations when applied to SPD matrix estimation in neuroimaging contexts. A critical challenge arises in modeling brain connectivity networks characterized by small-world topologies with densely interconnected hub regions. Sparse estimators systematically underestimate the strength of these prevalent dense connections due to their inherent structural bias toward parsimonious representations [202].

A further critical challenge in covariance estimation arises from outliers and artifacts contaminating neuroimaging time series. Such disturbances—from eye movements and muscle activity in EEG to head motion artifacts in fMRI—fundamentally violate the classical Gaussian assumption, often resulting in heavy-tailed distributions that deviate significantly from normality and render standard estimators statistically inconsistent. To address these issues, robust estimation frameworks, such as M-estimation, have been developed as flexible and outlier-resistant methodologies [203]. Notably, the Tyler estimator among them is distributionally robust and remains consistent under all elliptically symmetric distributions, including Gaussian, Student-t, and other heavy-tailed elliptical distributions [204], [205]. However, despite these theoretical advantages, its practical adoption has been hindered by restrictive underlying assumptions.

The challenges are compounded by the nonstationary nature of neuroimaging signals, where temporal variations in covariance structures degrade estimation fidelity and propagate errors to downstream classification tasks. To improve stability, domain-specific regularization techniques—such as shrinkage estimation and diagonal loading—have been strategically employed, enhancing discriminative classifier performance by refining covariance feature representations [206]–[208]. Notably, information geometry has emerged as a transformative paradigm, enabling direct analysis of covariance matrices as elements of the SPD manifold [209]. Geometric frameworks now provide theoretically grounded methods for both estimation and classification. For instance, recent advances leverage manifold-constrained optimization—including geodesic averaging and Riemannian online learning—to achieve robustness against nonstationary covariance drift [210]–[212].

7.2 Matrix Computation

Two significant computational challenges in *SPD learning* warrant careful attention: the estimation of the Fréchet mean and the execution of high-dimensional matrix operations and backpropagation. These challenges substantially hinder computational efficiency, and as training datasets expand, their impact becomes even more pronounced—resulting in increased complexity, higher storage demands, and difficulties in scaling algorithms. Overcoming these obstacles is essential for advancing the field and ensuring reliable performance in large-scale applications.

7.2.1 Fréchet Mean Estimation

The Fréchet mean, defined as the point that minimizes the sum of squared distances to all data points, frequently

lacks a closed-form solution. In manifold-valued data analysis—especially within neural network-based architectures—computing the Fréchet mean is often required, which can impose significant computational overhead.

For SPD manifold-valued data, a closed-form Fréchet mean can be obtained under the log-Euclidean metric because the matrix logarithm transforms the manifold into a vector space. In contrast, no closed-form solution exists under the affine-invariant Riemannian metric. Consequently, methods such as RieBN and its extensions [86], [92], [146] employ the Karcher flow algorithm with a fixed number of iterations per forward pass to approximate the Fréchet mean. Although fixing the number of iterations reduces the computational burden, it may not always converge to the exact Fréchet mean, potentially compromising accuracy.

Therefore, developing robust Fréchet mean estimators that maintain accuracy in noisy environments is a critical area of focus. In this regard, the power mean presents a promising alternative, as they exhibit greater resilience to noise compared to traditional gradient descent methods [213], and they also allow for efficient computation through multiplicative formulations.

7.2.2 High-Dimensional Issues

Matrix operations—such as inversion, square roots, and logarithms—create a significant computational bottleneck, particularly for large matrices, due to their cubic complexity with respect to dimensionality. In addition, in geometric deep learning, structured layers like BiMap, ReEig, and LogEig in SPDNet rely on matrix calculus for backpropagation [90]. As a result, these operations are computationally intensive, given the inherent challenges in computing matrix derivatives in high-dimensional settings [86].

To mitigate computational costs and enhance efficiency, researchers have explored two main strategies. The first strategy employs dimensionality reduction and clustering techniques to decrease data dimensionality, thereby lowering computational demands [74], [75], [111], [214], [215]. However, this approach may incur the information loss of raw neuroimaging data and then undermine the performance in the downstream tasks. The second strategy focuses on developing approximate methods and efficient algorithms for specific operations—such as matrix square roots and inverse square roots—applied during both forward and backward passes [90], [213], [216]–[219]. Although these methods reduce computational complexity, they often involve trade-offs between efficiency and accuracy, requiring careful evaluation in practical applications.

7.3 Interpretation

Interpreting the outcomes of neuroimaging decoding methods—especially those within the *SPD learning* framework—requires bridging a critical gap between model parameters and neurophysiologically meaningful patterns across spatial, temporal, and spectral domains. This involves identifying task-relevant brain regions, sensor channels, frequency bands, and temporal intervals, a challenge that has spurred the development of various attribution approaches [220]–[223]. While linear decoders often enable direct localization of neural sources through parameter

analysis [224], [225], nonlinear decoders operating on SPD manifolds face difficulties in intuitively mapping tangent space parameters to sensor-level neural patterns, which limits their overall interpretability. To address this, recent EEG decoding methods [226], [227] leverage transformations that project tangent space decoder weights into interpretable spatial and spectral patterns aligned with M/EEG channel topographies. Nevertheless, translating covariance features from diverse neuroimaging data into neurophysiologically grounded explanations remains an open frontier.

8 CONCLUSIONS

This review consolidates two decades of advancements in geometric methods for neuroimaging under the unified *SPD learning* framework. By rigorously modeling neuroimaging data—such as fMRI connectivity matrices, EEG/MEG/ECOG spatial covariance matrices, DTI diffusion tensors, and MRI deformation tensors—on SPD manifolds, *SPD learning* provides a mathematically coherent paradigm that preserves the intrinsic symmetry and positive definiteness of covariance structures while improving computational accuracy.

The review organizes geometric perspectives from Riemannian geometry, SPD manifolds, and geometric statistics, and classifies methodological advances into two main categories: geometric shallow learning—which includes tangent space projection, kernel methods, manifold learning, and information geometry—and geometric deep learning, exemplified by the SPDNet and gyrovector space approaches. It further categorizes neuroimaging applications into eight distinct domains and, through a systematic review of 55 seminal studies, demonstrates how *SPD learning* effectively addresses domain-specific challenges. To facilitate practical implementation, we also catalog core algorithmic components, including manifold-valued optimizers for geometric methods and 15 open-source packages for implementation.

However, several critical challenges must be addressed for *SPD learning* to reach its full potential. First, covariance estimation for covariance features is usually complicated by outliers, nonstationary signals, and violations of the Gaussian assumption, requiring the use of regularization techniques, robust estimators, or information-geometric frameworks. Second, the high computational complexity of matrix operations in high-dimensional settings makes the estimation of the Fréchet mean, as well as the execution of matrix operations and backpropagation, particularly challenging, and these difficulties can propagate errors to downstream tasks. Third, a neurophysiologically grounded interpretability framework for *SPD learning* models is still in its infancy. We review numerous studies to inspire readers to address these challenges, though practical deployment still remains constrained in each specific neuroimaging task.

By overcoming these challenges, *SPD learning* will unlock new possibilities for more accurate, efficient, and interpretable neuroimaging analyses, ultimately advancing both theoretical research and real-world applications. As methodological innovations continue to refine *SPD learning*, it will drive transformative progress in neuroimaging, brain-computer interfaces, and clinical diagnostics.

REFERENCES

- [1] J. Müller-Gerking, G. Pfurtscheller, and H. Flyvbjerg, “Designing optimal spatial filters for single-trial eeg classification in a movement task,” *Clinical neurophysiology*, vol. 110, no. 5, pp. 787–798, 1999.
- [2] D. O. Bos *et al.*, “Eeg-based emotion recognition,” *The influence of visual and auditory stimuli*, vol. 56, no. 3, pp. 1–17, 2006.
- [3] M. P. Van Den Heuvel and H. E. H. Pol, “Exploring the brain network: a review on resting-state fmri functional connectivity,” *European neuropsychopharmacology*, vol. 20, no. 8, pp. 519–534, 2010.
- [4] M. J. Brookes, J. R. Hale, J. M. Zumer, C. M. Stevenson, S. T. Francis, G. R. Barnes, J. P. Owen, P. G. Morris, and S. S. Nagarajan, “Measuring functional connectivity using meg: methodology and comparison with fmri,” *NeuroImage*, vol. 56, no. 3, pp. 1082–1104, 2011.
- [5] J.-M. Schoffelen and J. Gross, “Source connectivity analysis with meg and eeg,” *Human brain mapping*, vol. 30, no. 6, pp. 1857–1865, 2009.
- [6] N. Xu, P. C. Doerschuk, S. D. Keilholz, and R. N. Spreng, “Spatiotemporal functional interactivity among large-scale brain networks,” *NeuroImage*, vol. 227, p. 117628, 2021.
- [7] P. T. Fletcher, C. Lu, S. M. Pizer, and S. Joshi, “Principal geodesic analysis for the study of nonlinear statistics of shape,” *IEEE transactions on medical imaging*, vol. 23, no. 8, pp. 995–1005, 2004.
- [8] P. T. Fletcher and S. Joshi, “Riemannian geometry for the statistical analysis of diffusion tensor data,” *Signal Processing*, vol. 87, no. 2, pp. 250–262, 2007.
- [9] L. T. Skovgaard, “A riemannian geometry of the multivariate normal model,” *Scandinavian journal of statistics*, pp. 211–223, 1984.
- [10] X. Pennec, P. Fillard, and N. Ayache, “A riemannian framework for tensor computing,” *International Journal of computer vision*, vol. 66, no. 1, pp. 41–66, 2006.
- [11] X. Pennec, S. Sommer, and T. Fletcher, *Riemannian geometric statistics in medical image analysis*. Academic Press, 2019.
- [12] Y. Zhao, J. Su, Z. Yang, and Z. Ding, “A riemannian framework for functional clustering of whole brain white matter fibers,” in *2022 IEEE 19th International Symposium on Biomedical Imaging (ISBI)*. IEEE, 2022, pp. 1–5.
- [13] P. Fillard, X. Pennec, V. Arsigny, and N. Ayache, “Clinical dt-mri estimation, smoothing, and fiber tracking with log-euclidean metrics,” *IEEE transactions on medical imaging*, vol. 26, no. 11, pp. 1472–1482, 2007.
- [14] P. Khurd, R. Verma, and C. Davatzikos, “On characterizing and analyzing diffusion tensor images by learning their underlying manifold structure,” in *2006 Conference on Computer Vision and Pattern Recognition Workshop (CVPRW’06)*. IEEE, 2006, pp. 61–61.
- [15] Y. Zhao, Z. Yang, Z. Ding, and J. Su, “A riemannian framework for structurally curated functional clustering of brain white matter fibers,” *IEEE Transactions on Medical Imaging*, 2023.
- [16] N. Honnorat, S. Seshadri, R. Killiany, J. Blangero, D. C. Glahn, P. Fox, and M. Habes, “Riemannian frameworks for the harmonization of resting-state functional mri scans,” *Medical image analysis*, vol. 91, p. 103043, 2024.
- [17] G. Varoquaux, F. Baronnet, A. Kleinschmidt, P. Fillard, and B. Thirion, “Detection of brain functional-connectivity difference in post-stroke patients using group-level covariance modeling,” in *Medical Image Computing and Computer-Assisted Intervention—MICCAI 2010: 13th International Conference, Beijing, China, September 20–24, 2010, Proceedings, Part I 13*. Springer, 2010, pp. 200–208.
- [18] K. Dadi, M. Rahim, A. Abraham, D. Chyzyk, M. Milham, B. Thirion, G. Varoquaux, A. D. N. Initiative *et al.*, “Benchmarking functional connectome-based predictive models for resting-state fmri,” *NeuroImage*, vol. 192, pp. 115–134, 2019.
- [19] U. Pervaiz, D. Vidaurre, M. W. Woolrich, and S. M. Smith, “Optimising network modelling methods for fmri,” *NeuroImage*, vol. 211, p. 116604, 2020.
- [20] A. Barachant, S. Bonnet, M. Congedo, and C. Jutten, “Multiclass brain-computer interface classification by riemannian geometry,” *IEEE Transactions on Biomedical Engineering*, vol. 59, no. 4, pp. 920–928, 2011.
- [21] —, “Classification of covariance matrices using a riemannian-based kernel for bci applications,” *Neurocomputing*, vol. 112, pp. 172–178, 2013.
- [22] M. Congedo, A. Barachant, and R. Bhatia, “Riemannian geometry for eeg-based brain-computer interfaces; a primer and a review,” *Brain-Computer Interfaces*, vol. 4, no. 3, pp. 155–174, 2017.

- [23] F. Yger, M. Berar, and F. Lotte, "Riemannian Approaches in Brain-Computer Interfaces: A Review," *IEEE Transactions on Neural Systems and Rehabilitation Engineering*, vol. 25, no. 10, pp. 1753–1762, 2017.
- [24] G. Pfurtscheller and F. L. Da Silva, "Event-related eeg/meg synchronization and desynchronization: basic principles," *Clinical neurophysiology*, vol. 110, no. 11, pp. 1842–1857, 1999.
- [25] G. Pfurtscheller and C. Neuper, "Motor imagery and direct brain-computer communication," *Proceedings of the IEEE*, vol. 89, no. 7, pp. 1123–1134, 2001.
- [26] B. Blankertz, R. Tomioka, S. Lemm, M. Kawanabe, and K.-R. Muller, "Optimizing spatial filters for robust eeg single-trial analysis," *IEEE Signal processing magazine*, vol. 25, no. 1, pp. 41–56, 2007.
- [27] L. Yao, B. Zhu, and M. Shoaran, "Fast and accurate decoding of finger movements from ecog through riemannian features and modern machine learning techniques," *Journal of Neural Engineering*, vol. 19, no. 1, p. 016037, 2022.
- [28] M. Congedo, A. Barachant, and A. Andreev, "A new generation of brain-computer interface based on riemannian geometry," *arXiv preprint arXiv:1310.8115*, 2013.
- [29] B. Thirion, G. Varoquaux, E. Dohmatob, and J.-B. Poline, "Which fmri clustering gives good brain parcellations?" *Frontiers in neuroscience*, vol. 8, p. 167, 2014.
- [30] M. Teplan *et al.*, "Fundamentals of eeg measurement," *Measurement science review*, vol. 2, no. 2, pp. 1–11, 2002.
- [31] F. L. da Silva, "Eeg and meg: relevance to neuroscience," *Neuron*, vol. 80, no. 5, pp. 1112–1128, 2013.
- [32] G. Buzsáki, C. A. Anastassiou, and C. Koch, "The origin of extracellular fields and currents—eeg, ecog, lfp and spikes," *Nature reviews neuroscience*, vol. 13, no. 6, pp. 407–420, 2012.
- [33] R. L. Buckner, F. M. Krienen, and B. T. Yeo, "Opportunities and limitations of intrinsic functional connectivity mri," *Nature neuroscience*, vol. 16, no. 7, pp. 832–837, 2013.
- [34] K. J. Friston, "Functional and effective connectivity in neuroimaging: a synthesis," *Human brain mapping*, vol. 2, no. 1-2, pp. 56–78, 1994.
- [35] P. J. Basser, J. Mattiello, and D. LeBihan, "Mr diffusion tensor spectroscopy and imaging," *Biophysical journal*, vol. 66, no. 1, pp. 259–267, 1994.
- [36] E. O. Stejskal and J. E. Tanner, "Spin diffusion measurements: spin echoes in the presence of a time-dependent field gradient," *The journal of chemical physics*, vol. 42, no. 1, pp. 288–292, 1965.
- [37] D. W. McRobbie, E. A. Moore, M. J. Graves, and M. R. Prince, *MRI from Picture to Proton*. Cambridge university press, 2017.
- [38] W. Chen, S.-S. Chern, and K. S. Lam, *Lectures on differential geometry*. World Scientific Publishing Company, 1999, vol. 1.
- [39] P. Petersen, *Riemannian geometry*. Springer, 2006, vol. 171.
- [40] J. Jost, *Riemannian geometry and geometric analysis*. Springer, 2008, vol. 42005.
- [41] V. Arsigny, P. Fillard, X. Pennec, and N. Ayache, "Fast and simple computations on tensors with log-euclidean metrics." Ph.D. dissertation, INRIA, 2005.
- [42] —, "Log-euclidean metrics for fast and simple calculus on diffusion tensors," *Magnetic Resonance in Medicine: An Official Journal of the International Society for Magnetic Resonance in Medicine*, vol. 56, no. 2, pp. 411–421, 2006.
- [43] H. Karcher, "Riemannian center of mass and mollifier smoothing," *Communications on pure and applied mathematics*, vol. 30, no. 5, pp. 509–541, 1977.
- [44] M. Moakher, "A differential geometric approach to the geometric mean of symmetric positive-definite matrices," *SIAM journal on matrix analysis and applications*, vol. 26, no. 3, pp. 735–747, 2005.
- [45] F. Bouchard, A. Breloy, A. Collas, A. Renaux, and G. Ginolhac, "The fisher-rao geometry of ces distributions," in *Elliptically Symmetric Distributions in Signal Processing and Machine Learning*. Springer, 2024, pp. 37–77.
- [46] I. L. Dryden, A. Koloydenko, and D. Zhou, "Non-euclidean statistics for covariance matrices, with applications to diffusion tensor imaging," 2009.
- [47] S. Sra, "A new metric on the manifold of kernel matrices with application to matrix geometric means," *Advances in neural information processing systems*, vol. 25, 2012.
- [48] Z. Lin, "Riemannian geometry of symmetric positive definite matrices via cholesky decomposition," *SIAM Journal on Matrix Analysis and Applications*, vol. 40, no. 4, pp. 1353–1370, 2019.
- [49] L. Malagò, L. Montrucchio, and G. Pistone, "Wasserstein riemannian geometry of gaussian densities," *Information Geometry*, vol. 1, pp. 137–179, 2018.
- [50] R. Bhatia, T. Jain, and Y. Lim, "On the bures-wasserstein distance between positive definite matrices," *Expositiones Mathematicae*, vol. 37, no. 2, pp. 165–191, 2019.
- [51] C. Mostajeran, N. Da Costa, G. Van Goffrier, and R. Sepulchre, "Differential geometry with extreme eigenvalues in the positive semidefinite cone," *SIAM Journal on Matrix Analysis and Applications*, vol. 45, no. 2, pp. 1089–1113, 2024.
- [52] T. Fletcher, "Geodesic regression on riemannian manifolds," in *Proceedings of the Third International Workshop on Mathematical Foundations of Computational Anatomy-Geometrical and Statistical Methods for Modelling Biological Shape Variability*, 2011, pp. 75–86.
- [53] D. Grady and M. Kipp, "Geometric statistics and dynamic fragmentation," *Journal of Applied Physics*, vol. 58, no. 3, pp. 1210–1222, 1985.
- [54] X. Pennec, "Intrinsic statistics on riemannian manifolds: Basic tools for geometric measurements," *Journal of Mathematical Imaging and Vision*, vol. 25, pp. 127–154, 2006.
- [55] S. N. Chiu, D. Stoyan, W. S. Kendall, and J. Mecke, *Stochastic geometry and its applications*. John Wiley & Sons, 2013.
- [56] M. Zhang and P. T. Fletcher, "Probabilistic principal geodesic analysis," *Advances in neural information processing systems*, vol. 26, 2013.
- [57] M. Fréchet, "Les éléments aléatoires de nature quelconque dans un espace distancié," in *Annales de l'institut Henri Poincaré*, vol. 10, no. 4, 1948, pp. 215–310.
- [58] K. Grove and H. Karcher, "How to conjugate c 1-close group actions," *Mathematische Zeitschrift*, vol. 132, no. 1, pp. 11–20, 1973.
- [59] B. Afsari, "Riemannian l^p center of mass: existence, uniqueness, and convexity," *Proceedings of the American Mathematical Society*, vol. 139, no. 2, pp. 655–673, 2011.
- [60] S. Said, L. Bombrun, Y. Berthoumieu, and J. H. Manton, "Riemannian gaussian distributions on the space of symmetric positive definite matrices," *IEEE Transactions on Information Theory*, vol. 63, no. 4, pp. 2153–2170, 2017.
- [61] S. Said, N. Courty, N. Le Bihan, and S. J. Sangwine, "Exact principal geodesic analysis for data on $so(3)$," in *2007 15th European signal processing conference*. IEEE, 2007, pp. 1701–1705.
- [62] S. Sommer, F. Lauze, S. Hauberg, and M. Nielsen, "Manifold valued statistics, exact principal geodesic analysis and the effect of linear approximations," in *Computer Vision-ECCV 2010: 11th European Conference on Computer Vision, Heraklion, Crete, Greece, September 5-11, 2010, Proceedings, Part VI 11*. Springer, 2010, pp. 43–56.
- [63] P. T. Fletcher, "Geodesic regression and the theory of least squares on riemannian manifolds," *International journal of computer vision*, vol. 105, pp. 171–185, 2013.
- [64] H. J. Kim, N. Adluru, M. D. Collins, M. K. Chung, B. B. Bendlin, S. C. Johnson, R. J. Davidson, and V. Singh, "Multivariate general linear models (mgm) on riemannian manifolds with applications to statistical analysis of diffusion weighted images," in *Proceedings of the IEEE Conference on Computer Vision and Pattern Recognition*, 2014, pp. 2705–2712.
- [65] N. Lepore, C. Brun, Y.-Y. Chou, M.-C. Chiang, R. A. Dutton, K. M. Hayashi, E. Luders, O. L. Lopez, H. J. Aizenstein, A. W. Toga *et al.*, "Generalized tensor-based morphometry of hiv/aids using multivariate statistics on deformation tensors," *IEEE transactions on medical imaging*, vol. 27, no. 1, pp. 129–141, 2007.
- [66] S. Jayasumana, R. Hartley, M. Salzmann, H. Li, and M. Harandi, "Kernel methods on the riemannian manifold of symmetric positive definite matrices," in *proceedings of the IEEE Conference on Computer Vision and Pattern Recognition*, 2013, pp. 73–80.
- [67] S.-I. Amari, "Natural gradient works efficiently in learning," *Neural computation*, vol. 10, no. 2, pp. 251–276, 1998.
- [68] S.-i. Amari and H. Nagaoka, *Methods of information geometry*. American Mathematical Soc., 2000, vol. 191.
- [69] S.-i. Amari, *Information geometry and its applications*. Springer, 2016, vol. 194.
- [70] F. Nielsen, "An elementary introduction to information geometry," *Entropy*, vol. 22, no. 10, p. 1100, 2020.
- [71] J. B. Tenenbaum, V. d. Silva, and J. C. Langford, "A global geometric framework for nonlinear dimensionality reduction," *science*, vol. 290, no. 5500, pp. 2319–2323, 2000.

- [72] S. T. Roweis and L. K. Saul, "Nonlinear dimensionality reduction by locally linear embedding," *science*, vol. 290, no. 5500, pp. 2323–2326, 2000.
- [73] M. Belkin and P. Niyogi, "Laplacian eigenmaps for dimensionality reduction and data representation," *Neural computation*, vol. 15, no. 6, pp. 1373–1396, 2003.
- [74] M. T. Harandi, M. Salzmann, and R. Hartley, "From manifold to manifold: Geometry-aware dimensionality reduction for spd matrices," in *Computer Vision—ECCV 2014: 13th European Conference, Zurich, Switzerland, September 6–12, 2014, Proceedings, Part II* 13. Springer, 2014, pp. 17–32.
- [75] M. Harandi, M. Salzmann, and R. Hartley, "Dimensionality reduction on spd manifolds: The emergence of geometry-aware methods," *IEEE transactions on pattern analysis and machine intelligence*, vol. 40, no. 1, pp. 48–62, 2017.
- [76] O. Tuzel, F. Porikli, and P. Meer, "Pedestrian detection via classification on riemannian manifolds," *IEEE transactions on pattern analysis and machine intelligence*, vol. 30, no. 10, pp. 1713–1727, 2008.
- [77] D. Sabbagh, P. Ablin, G. Varoquaux, A. Gramfort, and D. A. Engemann, "Manifold-regression to predict from meg/eeg brain signals without source modeling," *Advances in Neural Information Processing Systems*, vol. 32, 2019.
- [78] —, "Predictive regression modeling with meg/eeg: from source power to signals and cognitive states," *NeuroImage*, vol. 222, p. 116893, 2020.
- [79] A. Mellot, A. Collas, P. L. Rodrigues, D. Engemann, and A. Gramfort, "Harmonizing and aligning m/eeg datasets with covariance-based techniques to enhance predictive regression modeling," *Imaging Neuroscience*, vol. 1, pp. 1–23, 2023.
- [80] M. M. Bronstein, J. Bruna, Y. LeCun, A. Szlam, and P. Vandergheynst, "Geometric deep learning: going beyond euclidean data," *IEEE Signal Processing Magazine*, vol. 34, no. 4, pp. 18–42, 2017.
- [81] R. J. Townshend, S. Eismann, A. M. Watkins, R. Rangan, M. Karelina, R. Das, and R. O. Dror, "Geometric deep learning of rna structure," *Science*, vol. 373, no. 6558, pp. 1047–1051, 2021.
- [82] K. Atz, F. Grisoni, and G. Schneider, "Geometric deep learning on molecular representations," *Nature Machine Intelligence*, vol. 3, no. 12, pp. 1023–1032, 2021.
- [83] J. Pineda, B. Midtvedt, H. Bachimanchi, S. Noé, D. Midtvedt, G. Volpe, and C. Manzo, "Geometric deep learning reveals the spatiotemporal features of microscopic motion," *Nature Machine Intelligence*, vol. 5, no. 1, pp. 71–82, 2023.
- [84] A. Bessadok, M. A. Mahjoub, and I. Reikik, "Graph neural networks in network neuroscience," *IEEE Transactions on Pattern Analysis and Machine Intelligence*, vol. 45, no. 5, pp. 5833–5848, 2023.
- [85] Z. Huang and L. V. Gool, "A Riemannian Network for SPD Matrix Learning," in *Proceedings of the Thirty-First AAAI Conference on Artificial Intelligence*, ser. AAAI'17. AAAI Press, 2017, pp. 2036–2042, event-place: San Francisco, California, USA.
- [86] D. Brooks, O. Schwander, F. Barbaresco, J.-Y. Schneider, and M. Cord, "Riemannian batch normalization for spd neural networks," *Advances in Neural Information Processing Systems*, vol. 32, 2019.
- [87] X. S. Nguyen, "Geomnet: A neural network based on riemannian geometries of spd matrix space and cholesky space for 3d skeleton-based interaction recognition," in *Proceedings of the IEEE/CVF International Conference on Computer Vision*, 2021, pp. 13 379–13 389.
- [88] S. Bonnabel, "Stochastic gradient descent on riemannian manifolds," *IEEE Transactions on Automatic Control*, vol. 58, no. 9, pp. 2217–2229, 2013.
- [89] G. Becigneul and O.-E. Ganea, "Riemannian adaptive optimization methods," in *International Conference on Learning Representations*, 2019.
- [90] C. Ionescu, O. Vantzios, and C. Sminchisescu, "Matrix backpropagation for deep networks with structured layers," in *Proceedings of the IEEE international conference on computer vision*, 2015, pp. 2965–2973.
- [91] R. Kobler, J.-i. Hirayama, Q. Zhao, and M. Kawanabe, "SPD domain-specific batch normalization to crack interpretable unsupervised domain adaptation in EEG," in *Advances in Neural Information Processing Systems*, S. Koyejo, S. Mohamed, A. Agarwal, D. Belgrave, K. Cho, and A. Oh, Eds., vol. 35. Curran Associates, Inc., 2022, pp. 6219–6235.
- [92] R. J. Kobler, J.-i. Hirayama, and M. Kawanabe, "Controlling The Fréchet Variance Improves Batch Normalization on the Symmetric Positive Definite Manifold," in *ICASSP 2022 - 2022 IEEE International Conference on Acoustics, Speech and Signal Processing (ICASSP)*. Singapore, Singapore: IEEE, 2022, pp. 3863–3867.
- [93] S. Santurkar, D. Tsipras, A. Ilyas, and A. Madry, "How Does Batch Normalization Help Optimization?" in *Proceedings of the 32nd International Conference on Neural Information Processing Systems*, ser. NIPS'18. Red Hook, NY, USA: Curran Associates Inc., 2018, pp. 2488–2498, event-place: Montréal, Canada.
- [94] Z. Chen, Y. Song, Y. Liu, and N. Sebe, "A lie group approach to riemannian normalization for SPD neural networks," in *The Twelfth International Conference on Learning Representations*, 2024.
- [95] A. A. Ungar, *Analytic hyperbolic geometry and Albert Einstein's special theory of relativity*. World Scientific, 2008.
- [96] A. Ungar, *A gyrovector space approach to hyperbolic geometry*. Springer Nature, 2022.
- [97] F. López, B. Pozzetti, S. Trettel, M. Strube, and A. Wienhard, "Vector-valued distance and gyrocalculus on the space of symmetric positive definite matrices," *Advances in Neural Information Processing Systems*, vol. 34, pp. 18 350–18 366, 2021.
- [98] X. S. Nguyen, "The gyro-structure of some matrix manifolds," *Advances in Neural Information Processing Systems*, vol. 35, pp. 26 618–26 630, 2022.
- [99] X. S. Nguyen and S. Yang, "Building neural networks on matrix manifolds: A gyrovector space approach," in *International Conference on Machine Learning*. PMLR, 2023, pp. 26 031–26 062.
- [100] X. S. Nguyen, S. Yang, and A. Histace, "Matrix manifold neural networks++," in *The Twelfth International Conference on Learning Representations*, 2024.
- [101] Anonymous, "Gyroatt: A gyro attention framework for matrix manifolds," in *Submitted to The Thirteenth International Conference on Learning Representations*, 2024, under review.
- [102] A. Barachant, S. Bonnet, M. Congedo, and C. Jutten, "Common spatial pattern revisited by riemannian geometry," in *2010 IEEE International Workshop on Multimedia Signal Processing*. IEEE, 2010, pp. 472–476.
- [103] F. Yger, M. Berar, and F. Lotte, "Riemannian approaches in brain-computer interfaces: a review," *IEEE Transactions on Neural Systems and Rehabilitation Engineering*, vol. 25, no. 10, pp. 1753–1762, 2016.
- [104] P. L. C. Rodrigues, C. Jutten, and M. Congedo, "Riemannian procrustes analysis: Transfer learning for brain-computer interfaces," *IEEE Transactions on Biomedical Engineering*, vol. 66, no. 8, pp. 2390–2401, 2018.
- [105] O. Yair, M. Ben-Chen, and R. Talmon, "Parallel transport on the cone manifold of spd matrices for domain adaptation," *IEEE Transactions on Signal Processing*, vol. 67, no. 7, pp. 1797–1811, 2019.
- [106] P. L. Rodrigues, M. Congedo, and C. Jutten, "Dimensionality transcending: a method for merging bci datasets with different dimensionalities," *IEEE Transactions on Biomedical Engineering*, vol. 68, no. 2, pp. 673–684, 2020.
- [107] A. Lahav and R. Talmon, "Procrustes analysis on the manifold of spd matrices for data sets alignment," *IEEE Transactions on Signal Processing*, 2023.
- [108] A. Mellot, A. Collas, S. Chevallier, D. A. Engemann, and A. Gramfort, "Physics-informed and unsupervised riemannian domain adaptation for machine learning on heterogeneous EEG datasets," in *32nd European Signal Processing Conference, EUSIPCO 2024, Lyon, France, August 26–30, 2024*. IEEE, 2024, pp. 1367–1371.
- [109] C. Bonet, B. Malézieux, A. Rakotomamonjy, L. Drumetz, T. Moreau, M. Kowalski, and N. Courty, "Sliced-wasserstein on symmetric positive definite matrices for m/eeg signals," in *International Conference on Machine Learning*. PMLR, 2023, pp. 2777–2805.
- [110] M. Congedo, P. L. C. Rodrigues, F. Bouchard, A. Barachant, and C. Jutten, "A closed-form unsupervised geometry-aware dimensionality reduction method in the riemannian manifold of spd matrices," in *2017 39th Annual International Conference of the IEEE Engineering in Medicine and Biology Society (EMBC)*. IEEE, 2017, pp. 3198–3201.
- [111] P. L. C. Rodrigues, F. Bouchard, M. Congedo, and C. Jutten, "Dimensionality reduction for bci classification using riemannian geometry," in *BCI 2017-7th International Brain-Computer Interface Conference*, 2017.
- [112] A. Davoudi, S. S. Ghidary, and K. Sadatnejad, "Dimensionality reduction based on distance preservation to local mean for symmetric positive definite matrices and its application in brain-computer interfaces," *Journal of neural engineering*, vol. 14, no. 3, p. 036019, 2017.

- [113] W. Samek, D. Blythe, K.-R. Müller, and M. Kawanabe, "Robust spatial filtering with beta divergence," *Advances in Neural Information Processing Systems*, vol. 26, 2013.
- [114] W. Samek, M. Kawanabe, and K.-R. Müller, "Divergence-based framework for common spatial patterns algorithms," *IEEE Reviews in Biomedical Engineering*, vol. 7, pp. 50–72, 2013.
- [115] Y.-J. Suh and B. H. Kim, "Riemannian embedding banks for common spatial patterns with eeg-based spd neural networks," in *Proceedings of the AAAI Conference on Artificial Intelligence*, vol. 35, no. 1, 2021, pp. 854–862.
- [116] C. Ju and C. Guan, "Tensor-cspnet: A novel geometric deep learning framework for motor imagery classification," *IEEE Transactions on Neural Networks and Learning Systems*, vol. 34, no. 12, pp. 10955–10969, 2023.
- [117] Y.-T. Pan, J.-L. Chou, and C.-S. Wei, "Matt: a manifold attention network for eeg decoding," *Advances in Neural Information Processing Systems*, vol. 35, pp. 31116–31129, 2022.
- [118] C. Ju and C. Guan, "Graph neural networks on spd manifolds for motor imagery classification: A perspective from the time-frequency analysis," *IEEE Transactions on Neural Networks and Learning Systems*, vol. 35, no. 12, pp. 17701–17715, 2024.
- [119] —, "Deep optimal transport for domain adaptation on spd manifolds," *Artificial Intelligence*, 2025.
- [120] C. Ju, D. Gao, R. Mane, B. Tan, Y. Liu, and C. Guan, "Federated transfer learning for eeg signal classification," in *2020 42nd annual international conference of the IEEE engineering in medicine & biology society (EMBC)*. IEEE, 2020, pp. 3040–3045.
- [121] D. Wilson, R. T. Schirrmester, L. A. Gemein, and T. Ball, "Deep riemannian networks for end-to-end eeg decoding," *Imaging Neuroscience*, 2025.
- [122] Y. Wang, S. Qiu, X. Ma, and H. He, "A prototype-based spd matrix network for domain adaptation eeg emotion recognition," *Pattern Recognition*, vol. 110, p. 107626, 2021.
- [123] E. K. Kalunga, S. Chevallier, Q. Barthélemy, K. Djouani, E. Monacelli, and Y. Hamam, "Online ssvep-based bci using riemannian geometry," *Neurocomputing*, vol. 191, pp. 55–68, 2016.
- [124] E. K. Kalunga, S. Chevallier, and Q. Barthélemy, "Transfer learning for ssvep-based bci using riemannian similarities between users," in *2018 26th European Signal Processing Conference (EUSIPCO)*. IEEE, 2018, pp. 1685–1689.
- [125] C. Ju, R. J. Kobler, L. Tang, C. Guan, and M. Kawanabe, "Deep geodesic canonical correlation analysis for covariance-based neuroimaging data," in *The Twelfth International Conference on Learning Representations*, 2024.
- [126] M. Dai, Z. Zhang, and A. Srivastava, "Analyzing dynamical brain functional connectivity as trajectories on space of covariance matrices," *IEEE transactions on medical imaging*, vol. 39, no. 3, pp. 611–620, 2019.
- [127] Z. Huang, H. Cai, T. Dan, Y. Lin, P. Laurienti, and G. Wu, "Detecting brain state changes by geometric deep learning of functional dynamics on riemannian manifold," in *Medical Image Computing and Computer Assisted Intervention—MICCAI 2021: 24th International Conference, Strasbourg, France, September 27–October 1, 2021, Proceedings, Part VII 24*. Springer, 2021, pp. 543–552.
- [128] T. Dan, Z. Huang, H. Cai, P. J. Laurienti, and G. Wu, "Learning brain dynamics of evolving manifold functional mri data using geometric-attention neural network," *IEEE Transactions on Medical Imaging*, vol. 41, no. 10, pp. 2752–2763, 2022.
- [129] T. Dan, Z. Huang, H. Cai, R. G. Lyday, P. J. Laurienti, and G. Wu, "Uncovering shape signatures of resting-state functional connectivity by geometric deep learning on riemannian manifold," *Human Brain Mapping*, vol. 43, no. 13, pp. 3970–3986, 2022.
- [130] T. Dan, Z. Wei, W. H. Kim, and G. Wu, "Exploring the enigma of neural dynamics through a scattering-transform mixer landscape for riemannian manifold," in *Forty-first International Conference on Machine Learning*, 2024.
- [131] D. A. Engemann, A. Mellot, R. Höchenberger, H. Banville, D. Sabbagh, L. Gemein, T. Ball, and A. Gramfort, "A reusable benchmark of brain-age prediction from m/eeg resting-state signals," *Neuroimage*, vol. 262, p. 119521, 2022.
- [132] A. Collas, R. Flamary, and A. Gramfort, "Weakly supervised covariance matrices alignment through stiefel matrices estimation for meg applications," *arXiv preprint arXiv:2402.03345*, 2024.
- [133] A. Mellot, A. Collas, S. Chevallier, A. Gramfort, and D. A. Engemann, "Geodesic optimization for predictive shift adaptation on eeg data," *Advances in Neural Information Processing Systems*, vol. 37, 2025.
- [134] A. Qiu, A. Lee, M. Tan, and M. K. Chung, "Manifold learning on brain functional networks in aging," *Medical image analysis*, vol. 20, no. 1, pp. 52–60, 2015.
- [135] F. Liem, G. Varoquaux, J. Kynast, F. Beyer, S. K. Masouleh, J. M. Huntenburg, L. Lampe, M. Rahim, A. Abraham, R. C. Craddock *et al.*, "Predicting brain-age from multimodal imaging data captures cognitive impairment," *Neuroimage*, vol. 148, pp. 179–188, 2017.
- [136] D. A. Engemann, O. Kozynets, D. Sabbagh, G. Lemaître, G. Varoquaux, F. Liem, and A. Gramfort, "Combining magnetoencephalography with magnetic resonance imaging enhances learning of surrogate-biomarkers," *Elife*, vol. 9, p. e54055, 2020.
- [137] B. Ng, M. Dressler, G. Varoquaux, J. B. Poline, M. Greicius, and B. Thirion, "Transport on riemannian manifold for functional connectivity-based classification," in *Medical Image Computing and Computer-Assisted Intervention—MICCAI 2014: 17th International Conference, Boston, MA, USA, September 14–18, 2014, Proceedings, Part II 17*. Springer, 2014, pp. 405–412.
- [138] B. Ng, G. Varoquaux, J. B. Poline, M. Greicius, and B. Thirion, "Transport on riemannian manifold for connectivity-based brain decoding," *IEEE transactions on medical imaging*, vol. 35, no. 1, pp. 208–216, 2015.
- [139] J.-B. Schiratti, S. Allasonniere, O. Colliot, and S. Durrleman, "Learning spatiotemporal trajectories from manifold-valued longitudinal data," *Advances in neural information processing systems*, vol. 28, 2015.
- [140] H. J. Kim, N. Adluru, H. Suri, B. C. Vemuri, S. C. Johnson, and V. Singh, "Riemannian nonlinear mixed effects models: Analyzing longitudinal deformations in neuroimaging," in *Proceedings of the IEEE conference on computer vision and pattern recognition*, 2017, pp. 2540–2549.
- [141] S. Gruffaz, P.-E. Poulet, E. Maheux, B. Jedynak, and S. Durrleman, "Learning riemannian metric for disease progression modeling," *Advances in Neural Information Processing Systems*, vol. 34, pp. 23780–23792, 2021.
- [142] J.-B. Schiratti, S. Allasonnière, O. Colliot, and S. Durrleman, "A bayesian mixed-effects model to learn trajectories of changes from repeated manifold-valued observations," *Journal of Machine Learning Research*, vol. 18, no. 133, pp. 1–33, 2017.
- [143] S. Jeong, W. Jung, J. Sohn, and H.-I. Suk, "Deep Geometric Learning With Monotonicity Constraints for Alzheimer's Disease Progression," *IEEE Transactions on Neural Networks and Learning Systems*, pp. 1–13, 2024.
- [144] C. Neuper, R. Scherer, M. Reiner, and G. Pfurtscheller, "Imagery of motor actions: Differential effects of kinesthetic and visual-motor mode of imagery in single-trial EEG," *Cognitive Brain Research*, vol. 25, no. 3, pp. 668–677, 2005.
- [145] B. Blankertz, S. Lemm, M. Treder, S. Haufe, and K.-R. Müller, "Single-trial analysis and classification of erp components—a tutorial," *NeuroImage*, vol. 56, no. 2, pp. 814–825, 2011.
- [146] R. Kobler, J.-i. Hirayama, Q. Zhao, and M. Kawanabe, "Spd domain-specific batch normalization to crack interpretable unsupervised domain adaptation in eeg," *Advances in Neural Information Processing Systems*, vol. 35, pp. 6219–6235, 2022.
- [147] D. Wilson, R. T. Schirrmester, L. A. W. Gemein, and T. Ball, "Deep Riemannian Networks for EEG Decoding," 2022.
- [148] F. Lotte, L. Bougrain, A. Cichocki, M. Clerc, M. Congedo, A. Rakotomamonjy, and F. Yger, "A review of classification algorithms for eeg-based brain-computer interfaces: a 10 year update," *Journal of neural engineering*, vol. 15, no. 3, p. 031005, 2018.
- [149] P. Zanini, M. Congedo, C. Jutten, S. Said, and Y. Berthoumieu, "Transfer learning: A riemannian geometry framework with applications to brain-computer interfaces," *IEEE Transactions on Biomedical Engineering*, vol. 65, no. 5, pp. 1107–1116, 2017.
- [150] A. Bleuzé, J. Mattout, and M. Congedo, "Tangent space alignment: Transfer learning for Brain-Computer Interface," *Frontiers in Human Neuroscience*, vol. 16, p. 1049985, Dec. 2022.
- [151] R. Jenke, A. Peer, and M. Buss, "Feature extraction and selection for emotion recognition from eeg," *IEEE Transactions on Affective Computing*, vol. 5, no. 3, pp. 327–339, 2014.
- [152] F.-B. Vialatte, M. Maurice, J. Dauwels, and A. Cichocki, "Steady-state visually evoked potentials: focus on essential paradigms and future perspectives," *Progress in neurobiology*, vol. 90, no. 4, pp. 418–438, 2010.
- [153] Z. Lin, C. Zhang, W. Wu, and X. Gao, "Frequency recognition based on canonical correlation analysis for ssvep-based bcis,"

- IEEE Transactions on Biomedical Engineering*, vol. 53, no. 12, pp. 2610–2614, 2006.
- [154] S. Waldert, T. Pistohl, C. Braun, T. Ball, A. Aertsen, and C. Mehring, “A review on directional information in neural signals for brain-machine interfaces,” *Journal of Physiology-Paris*, vol. 103, no. 3-5, pp. 244–254, 2009.
- [155] N. Luo, W. Shi, Z. Yang, M. Song, and T. Jiang, “Multimodal fusion of brain imaging data: Methods and applications,” *Machine Intelligence Research*, vol. 21, no. 1, pp. 136–152, 2024.
- [156] M. G. Philiastides, T. Tu, and P. Sajda, “Inferring Macroscale Brain Dynamics via Fusion of Simultaneous EEG-fMRI,” *Annual Review of Neuroscience*, vol. 44, no. 1, pp. 315–334, Jul. 2021.
- [157] T. Warbrick, “Simultaneous EEG-fMRI: What Have We Learned and What Does the Future Hold?” *Sensors*, vol. 22, no. 6, p. 2262, Mar. 2022.
- [158] B. He and Z. Liu, “Multimodal functional neuroimaging: integrating functional mri and eeg/meg,” *IEEE Reviews in Biomedical Engineering*, vol. 1, pp. 23–40, 2008.
- [159] M. Filippi, E. G. Spinelli, C. Cividini, and F. Agosta, “Resting state dynamic functional connectivity in neurodegenerative conditions: a review of magnetic resonance imaging findings,” *Frontiers in neuroscience*, vol. 13, p. 657, 2019.
- [160] Z. Zhang, J. Su, E. Klassen, H. Le, and A. Srivastava, “Rate-invariant analysis of covariance trajectories,” *Journal of Mathematical Imaging and Vision*, vol. 60, pp. 1306–1323, 2018.
- [161] L. K. Ferreira and G. F. Busatto, “Resting-state functional connectivity in normal brain aging,” *Neuroscience & Biobehavioral Reviews*, vol. 37, no. 3, pp. 384–400, 2013.
- [162] J. H. Cole and K. Franke, “Predicting age using neuroimaging: innovative brain ageing biomarkers,” *Trends in neurosciences*, vol. 40, no. 12, pp. 681–690, 2017.
- [163] M. G. Puxeddu, J. Faskowitz, R. F. Betzel, M. Petti, L. Astolfi, and O. Sporns, “The modular organization of brain cortical connectivity across the human lifespan,” *NeuroImage*, vol. 218, p. 116974, 2020.
- [164] F. Deligianni, G. Varoquaux, B. Thirion, E. Robinson, D. J. Sharp, A. D. Edwards, and D. Rueckert, “A probabilistic framework to infer brain functional connectivity from anatomical connections,” in *Information Processing in Medical Imaging: 22nd International Conference, IPMI 2011, Kloster Irsee, Germany, July 3-8, 2011. Proceedings 22*. Springer, 2011, pp. 296–307.
- [165] N. Yahata, J. Morimoto, R. Hashimoto, G. Lisi, K. Shibata, Y. Kawakubo, H. Kuwabara, M. Kuroda, T. Yamada, F. Megumi *et al.*, “A small number of abnormal brain connections predicts adult autism spectrum disorder,” *Nature communications*, vol. 7, no. 1, p. 11254, 2016.
- [166] N. Ichikawa, G. Lisi, N. Yahata, G. Okada, M. Takamura, R.-i. Hashimoto, T. Yamada, M. Yamada, T. Suhara, S. Moriguchi *et al.*, “Primary functional brain connections associated with melancholic major depressive disorder and modulation by antidepressants,” *Scientific reports*, vol. 10, no. 1, p. 3542, 2020.
- [167] Y. Yoshihara, G. Lisi, N. Yahata, J. Fujino, Y. Matsumoto, J. Miyata, G.-i. Sugihara, S.-i. Urayama, M. Kubota, M. Yamashita *et al.*, “Overlapping but asymmetrical relationships between schizophrenia and autism revealed by brain connectivity,” *Schizophrenia bulletin*, vol. 46, no. 5, pp. 1210–1218, 2020.
- [168] P. Diggle, *Analysis of longitudinal data*. Oxford university press, 2002.
- [169] C. R. Jack, D. S. Knopman, W. J. Jagust, L. M. Shaw, P. S. Aisen, M. W. Weiner, R. C. Petersen, and J. Q. Trojanowski, “Hypothetical model of dynamic biomarkers of the alzheimer’s pathological cascade,” *The Lancet Neurology*, vol. 9, no. 1, pp. 119–128, 2010.
- [170] P.-A. Absil, R. Mahony, and R. Sepulchre, *Optimization algorithms on matrix manifolds*. Princeton University Press, 2008.
- [171] N. Boumal, *An introduction to optimization on smooth manifolds*. Cambridge University Press, 2023.
- [172] H. Zhang and S. Sra, “First-order methods for geodesically convex optimization,” in *Conference on Learning Theory*. PMLR, 2016, pp. 1617–1638.
- [173] D. P. Kingma and J. Ba, “Adam: A method for stochastic optimization,” *arXiv preprint arXiv:1412.6980*, 2014.
- [174] J. Duchi, E. Hazan, and Y. Singer, “Adaptive subgradient methods for online learning and stochastic optimization,” *Journal of machine learning research*, vol. 12, no. 7, 2011.
- [175] S. J. Reddi, S. Kale, and S. Kumar, “On the convergence of adam and beyond,” *arXiv preprint arXiv:1904.09237*, 2019.
- [176] H. Zhang, S. J. Reddi, and S. Sra, “Riemannian svrg: Fast stochastic optimization on riemannian manifolds,” *Advances in Neural Information Processing Systems*, vol. 29, 2016.
- [177] W. Lin, V. Duruisseaux, M. Leok, F. Nielsen, M. E. Khan, and M. Schmidt, “Simplifying momentum-based positive-definite submanifold optimization with applications to deep learning,” in *International Conference on Machine Learning*. PMLR, 2023, pp. 21 026–21 050.
- [178] N. Boumal, B. Mishra, P.-A. Absil, and R. Sepulchre, “Manopt, a matlab toolbox for optimization on manifolds,” *Journal of Machine Learning Research*, vol. 15, no. 42, pp. 1455–1459, 2014.
- [179] J. Townsend, N. Koep, and S. Weichwald, “Pymanopt: A python toolbox for optimization on manifolds using automatic differentiation,” *Journal of Machine Learning Research*, vol. 17, no. 137, pp. 1–5, 2016.
- [180] R. Bergmann, “Manopt.jl: Optimization on manifolds in Julia,” *Journal of Open Source Software*, vol. 7, no. 70, p. 3866, 2022.
- [181] S. D. Axen, M. Baran, R. Bergmann, and K. Rzecki, “Manifolds.jl: An extensible julia framework for data analysis on manifolds,” *ACM Transactions on Mathematical Software*, vol. 49, no. 4, dec 2023.
- [182] M. Kochurov, R. Karimov, and S. Kozlukov, “Geopt: Riemannian optimization in pytorch,” 2020.
- [183] M. Lezcano-Casado, “Trivializations for gradient-based optimization on manifolds,” in *Advances in Neural Information Processing Systems, NeurIPS*, 2019, pp. 9154–9164.
- [184] N. Miolane, N. Guigui, A. L. Brigant, J. Mathe, B. Hou, Y. Thanwerdas, S. Heyder, O. Peltre, N. Koep, H. Zaatiti, H. Hajri, Y. Cabanes, T. Gerald, P. Chauchat, C. Shewmake, D. Brooks, B. Kainz, C. Donnat, S. Holmes, and X. Pennec, “Geomstats: A python package for riemannian geometry in machine learning,” *Journal of Machine Learning Research*, vol. 21, no. 223, pp. 1–9, 2020.
- [185] A. Le Brigant, J. Deschamps, A. Collas, and N. Miolane, “Parametric information geometry with the package geomstats,” *ACM Transactions on Mathematical Software*, vol. 49, no. 4, pp. 1–26, 2023.
- [186] A. Barachant, Q. Barthélemy, J.-R. King, A. Gramfort, S. Chevallier, P. L. C. Rodrigues, E. Olivetti, V. Goncharenko, G. W. vom Berg, G. Regui, A. Lebourrier, E. Bjäreholt, M. S. Yamamoto, P. Clisson, and M.-C. Corsi, “pyriemann/pyriemann: v0.5,” 2023.
- [187] F. Pedregosa, G. Varoquaux, A. Gramfort, V. Michel, B. Thirion, O. Grisel, M. Blondel, P. Prettenhofer, R. Weiss, V. Dubourg *et al.*, “Scikit-learn: Machine learning in python,” *the Journal of machine Learning research*, vol. 12, pp. 2825–2830, 2011.
- [188] A. Gramfort, M. Luessi, E. Larson, D. A. Engemann, D. Strohmeier, C. Brodbeck, R. Goj, M. Jas, T. Brooks, L. Parkkonen *et al.*, “Meg and eeg data analysis with mne-python,” *Frontiers in Neuroinformatics*, vol. 7, p. 267, 2013.
- [189] A. Abraham, F. Pedregosa, M. Eickenberg, P. Gervais, A. Mueller, J. Kossaifi, A. Gramfort, B. Thirion, and G. Varoquaux, “Machine learning for neuroimaging with scikit-learn,” *Frontiers in Neuroinformatics*, vol. 8, 2014.
- [190] P. J. Huber, *Robust statistics*. John Wiley & Sons, 2004, vol. 523.
- [191] B. D. Ripley, *Spatial statistics*. John Wiley & Sons, 2005.
- [192] M. A. Burock and A. M. Dale, “Estimation and detection of event-related fmri signals with temporally correlated noise: A statistically efficient and unbiased approach,” *Human brain mapping*, vol. 11, no. 4, pp. 249–260, 2000.
- [193] G. Derado, F. D. Bowman, and C. D. Kilts, “Modeling the spatial and temporal dependence in fmri data,” *Biometrics*, vol. 66, no. 3, pp. 949–957, 2010.
- [194] G. Varoquaux, A. Gramfort, J.-B. Poline, and B. Thirion, “Brain covariance selection: better individual functional connectivity models using population prior,” *Advances in neural information processing systems*, vol. 23, 2010.
- [195] O. Ledoit and M. Wolf, “Honey, i shrunk the sample covariance matrix,” *UPF economics and business working paper*, no. 691, 2003.
- [196] —, “A well-conditioned estimator for large-dimensional covariance matrices,” *Journal of multivariate analysis*, vol. 88, no. 2, pp. 365–411, 2004.
- [197] L. Wehbe, A. Ramdas, R. C. Steorts, and C. R. Shalizi, “Regularized brain reading with shrinkage and smoothing,” *The annals of applied statistics*, vol. 9, no. 4, p. 1997, 2015.
- [198] A. F. Mejia, M. B. Nebel, H. Shou, C. M. Crainiceanu, J. J. Pekar, S. Mostofsky, B. Caffo, and M. A. Lindquist, “Improving reliability of subject-level resting-state fmri parcellation with shrinkage estimators,” *NeuroImage*, vol. 112, pp. 14–29, 2015.

- [199] J. Höhne, D. Bartz, M. N. Hebart, K.-R. Müller, and B. Blankertz, "Analyzing neuroimaging data with subclasses: A shrinkage approach," *NeuroImage*, vol. 124, pp. 740–751, 2016.
- [200] M. Rahim, B. Thirion, and G. Varoquaux, "Population shrinkage of covariance (posce) for better individual brain functional-connectivity estimation," *Medical image analysis*, vol. 54, pp. 138–148, 2019.
- [201] J. Friedman, T. Hastie, and R. Tibshirani, "Sparse inverse covariance estimation with the graphical lasso," *Biostatistics*, vol. 9, no. 3, pp. 432–441, 2008.
- [202] G. Varoquaux, A. Gramfort, J. B. Poline, and B. Thirion, "Markov models for fmri correlation structure: is brain functional connectivity small world, or decomposable into networks?" *Journal of physiology-Paris*, vol. 106, no. 5–6, pp. 212–221, 2012.
- [203] R. A. Maronna, "Robust m-estimators of multivariate location and scatter," *The annals of statistics*, pp. 51–67, 1976.
- [204] D. E. Tyler, "A distribution-free m-estimator of multivariate scatter," *The annals of Statistics*, pp. 234–251, 1987.
- [205] Y. Sun, P. Babu, and D. P. Palomar, "Regularized tyler's scatter estimator: Existence, uniqueness, and algorithms," *IEEE Transactions on Signal Processing*, vol. 62, no. 19, pp. 5143–5156, 2014.
- [206] F. Lotte and C. Guan, "Regularizing common spatial patterns to improve bci designs: unified theory and new algorithms," *IEEE Transactions on Biomedical Engineering*, vol. 58, no. 2, pp. 355–362, 2010.
- [207] H. Lu, H.-L. Eng, C. Guan, K. N. Plataniotis, and A. N. Venetsanopoulos, "Regularized common spatial pattern with aggregation for eeg classification in small-sample setting," *IEEE transactions on Biomedical Engineering*, vol. 57, no. 12, pp. 2936–2946, 2010.
- [208] J. Olias, R. Martín-Clemente, M. A. Sarmiento-Vega, and S. Cruces, "Eeg signal processing in mi-bci applications with improved covariance matrix estimators," *IEEE Transactions on Neural Systems and Rehabilitation Engineering*, vol. 27, no. 5, pp. 895–904, 2019.
- [209] S. T. Smith, "Covariance, subspace, and intrinsic crame/spl acute/r-rao bounds," *IEEE Transactions on Signal Processing*, vol. 53, no. 5, pp. 1610–1630, 2005.
- [210] A. Wiesel, "Geodesic convexity and covariance estimation," *IEEE transactions on signal processing*, vol. 60, no. 12, pp. 6182–6189, 2012.
- [211] L. Ning, X. Jiang, and T. Georgiou, "On the geometry of covariance matrices," *IEEE Signal Processing Letters*, vol. 20, no. 8, pp. 787–790, 2013.
- [212] A. Musolas, S. T. Smith, and Y. Marzouk, "Geodesically parameterized covariance estimation," *SIAM Journal on Matrix Analysis and Applications*, vol. 42, no. 2, pp. 528–556, 2021.
- [213] M. Congedo, A. Barachant, and E. K. Koopaie, "Fixed Point Algorithms for Estimating Power Means of Positive Definite Matrices," *IEEE Transactions on Signal Processing*, vol. 65, no. 9, pp. 2211–2220, May 2017.
- [214] A. Goh and R. Vidal, "Clustering and dimensionality reduction on riemannian manifolds," in *2008 IEEE Conference on computer vision and pattern recognition*. IEEE, 2008, pp. 1–7.
- [215] F. P. Kalaganis, N. A. Laskaris, E. Chatzilaris, S. Nikolopoulos, and I. Kompatsiaris, "A riemannian geometry approach to reduced and discriminative covariance estimation in brain computer interfaces," *IEEE Transactions on Biomedical Engineering*, vol. 67, no. 1, pp. 245–255, 2019.
- [216] M. Engin, L. Wang, L. Zhou, and X. Liu, "Deepkspd: Learning kernel-matrix-based spd representation for fine-grained image recognition," in *Proceedings of the European Conference on Computer Vision (ECCV)*, 2018, pp. 612–627.
- [217] P. Li, J. Xie, Q. Wang, and Z. Gao, "Towards faster training of global covariance pooling networks by iterative matrix square root normalization," in *Proceedings of the IEEE conference on computer vision and pattern recognition*, 2018, pp. 947–955.
- [218] W. Wang, Z. Dang, Y. Hu, P. Fua, and M. Salzmann, "Robust Differentiable SVD," *IEEE Transactions on Pattern Analysis and Machine Intelligence*, pp. 1–1, 2021.
- [219] Y. Song, N. Sebe, and W. Wang, "Fast Differentiable Matrix Square Root and Inverse Square Root," *IEEE Transactions on Pattern Analysis and Machine Intelligence*, vol. 45, no. 6, pp. 7367–7380, Jun. 2023.
- [220] S. Bach, A. Binder, G. Montavon, F. Klauschen, K.-R. Müller, and W. Samek, "On Pixel-Wise Explanations for Non-Linear Classifier Decisions by Layer-Wise Relevance Propagation," *PLOS ONE*, vol. 10, no. 7, p. e0130140, Jul. 2015.
- [221] S. M. Lundberg and S.-I. Lee, "A unified approach to interpreting model predictions," in *Proceedings of the 31st International Conference on Neural Information Processing Systems*, ser. NIPS'17. Red Hook, NY, USA: Curran Associates Inc., 2017, pp. 4768–4777, event-place: Long Beach, California, USA.
- [222] M. Sundararajan, A. Taly, and Q. Yan, "Axiomatic attribution for deep networks," in *International conference on machine learning*. PMLR, 2017, pp. 3319–3328.
- [223] W. Samek, G. Montavon, A. Vedaldi, L. K. Hansen, and K.-R. Müller, Eds., *Explainable AI: Interpreting, Explaining and Visualizing Deep Learning*, ser. Lecture Notes in Computer Science. Cham: Springer International Publishing, 2019, vol. 11700.
- [224] S. Haufe, F. Meinecke, K. Görgen, S. Dähne, J.-D. Haynes, B. Blankertz, and F. Bießmann, "On the interpretation of weight vectors of linear models in multivariate neuroimaging," *Neuroimage*, vol. 87, pp. 96–110, 2014.
- [225] L. C. Parra, C. D. Spence, A. D. Gerson, and P. Sajda, "Recipes for the linear analysis of EEG," *NeuroImage*, vol. 28, no. 2, pp. 326–341, 2005, ISBN: 1053-8119 (Print).
- [226] J. Xu, M. Grosse-Wentrup, and V. Jayaram, "Tangent space spatial filters for interpretable and efficient riemannian classification," *Journal of Neural Engineering*, vol. 17, no. 2, p. 026043, 2020.
- [227] R. J. Kobler, J.-I. Hirayama, L. Hehenberger, C. Lopes-Dias, G. R. Müller-Putz, and M. Kawanabe, "On the interpretation of linear riemannian tangent space model parameters in m/eeg," in *2021 43rd Annual International Conference of the IEEE Engineering in Medicine & Biology Society (EMBC)*. IEEE, 2021, pp. 5909–5913.